8 Experimental Case No. 1

In this chapter, the experimental case no. 1, which was introduced in section 1.7.1 is described. This experimental case is based on the two-dimensional plane five storey frame structure illustrated in figure 1.2, and it is described how this structure is modelled and how the structural response is simulated. Finally, the simulation results are presented and analyzed. The analysis will concern the asymptotic properties of the PEM estimator armav.m of the STDI toolbox which is described in section 7.3. The asymptotic properties are the bias and the standard deviations of the modal parameters obtained from the estimated ARMAV models. These properties will be analysed as a function of record length and noise level. Further, the sampled standard deviations of the modal parameters will be compared with the estimated standard deviations obtained on the basis of the PEM estimate.

8.1 A Simulation Study of a Five Storey Structure

In this section, it will be shown how the structure is modelled in continuous time and converted to an equivalent discrete-time model. Finally, the modal properties of the structure are presented.

8.1.1 Modelling of the Structure

All mass of the plane frame structure is assumed to be concentrated in the horizontal beam elements of the structure, which implies that the centre of each of the beams is a mass-point. These elements are also assumed to be completely stiff, which implies that only horizontal displacements will be considered.

The horizontal motion of all mass-points is assumed to be observed and the five bending modes will be investigated. This implies that the displacements of the five storeys are described by the following second-order differential equation system, see section 3.1

$$\ddot{\boldsymbol{z}}(t) + \boldsymbol{M}^{-1}\boldsymbol{C}\dot{\boldsymbol{z}}(t) + \boldsymbol{M}^{-1}\boldsymbol{K}\boldsymbol{z}(t) = \boldsymbol{M}^{-1}\boldsymbol{f}(t) \qquad \textbf{(1)}$$

All system matrices have the same dimensions, and the structure is assumed to be excited at all mass-points by forces assembled in the vector $\boldsymbol{f}(t)$. The mass matrix is chosen as the identity matrix. A non-proportional damping matrix is assumed. This damping matrix is selected in such a way that the modes of the structure will be underdamped, with damping ratios around a few per cent. The mass-normalized damping and stiffness matrices are given by

$$\boldsymbol{M}^{-1}\boldsymbol{C} = 10^{0}\sec^{-1} \times \begin{bmatrix} 2.41 & -2.40 & 0 & 0 & 0 \\ -2.40 & 4.81 & -2.40 & 0 & 0 \\ 0 & -2.40 & 4.81 & -2.40 & 0 \\ 0 & 0 & -2.40 & 4.81 & -2.40 \\ 0 & 0 & 0 & -2.40 & 3.01 \end{bmatrix} \quad \textbf{(2)}$$

$$\boldsymbol{M}^{-1}\boldsymbol{K} = 10^{3}\sec^{-2} \times \begin{bmatrix} 4.80 & -4.80 & 0 & 0 & 0 \\ -4.80 & 9.60 & -4.80 & 0 & 0 \\ 0 & -4.80 & 9.60 & -4.80 & 0 \\ 0 & 0 & -4.80 & 9.60 & -4.80 \\ 0 & 0 & 0 & -4.80 & 6.00 \end{bmatrix} \quad \textbf{(3)}$$

The excitation of the system is assumed to be a continuous-time Gaussian white noise, described by the intensity matrix $\boldsymbol{W} = \boldsymbol{I}$.

8.1.2 Modal Properties of the Structure

The performance of the PEM routine armav.m will be tested on its ability to estimate the modal parameters. Therefore, the true modal parameters of the model will be presented in this section. These parameters are obtained by applying the techniques given in section 3.1 to (8.1). The modal parameters used in the analysis are:

- *Natural eigenfrequencies.*
- *Damping ratios.*
- *Scaled mode shapes.*

The mode shapes will be scaled so that they are unity at the first floor. This is a necessary step, in order to make sure that the numerical differentiation performed works properly, when the standard deviations of the mode shape coordinates are estimated. In this way the default scaling used by the MATLAB eigenvalue solver is interrupted.

The natural eigenfrequencies and damping ratios are shown in table 8.1. In figure 8.1 the magnitudes of the mode shapes are plotted. In table 8.2 and table 8.3 the magnitudes and phase angels are listed.

Mode No.	1	2	3	4	5
f_i [Hz]	2.141	7.590	13.292	17.970	21.003
ζ_i [%]	1.24	1.34	2.61	2.71	3.31

Table 8.1: Natural eigenfrequencies and damping ratios.

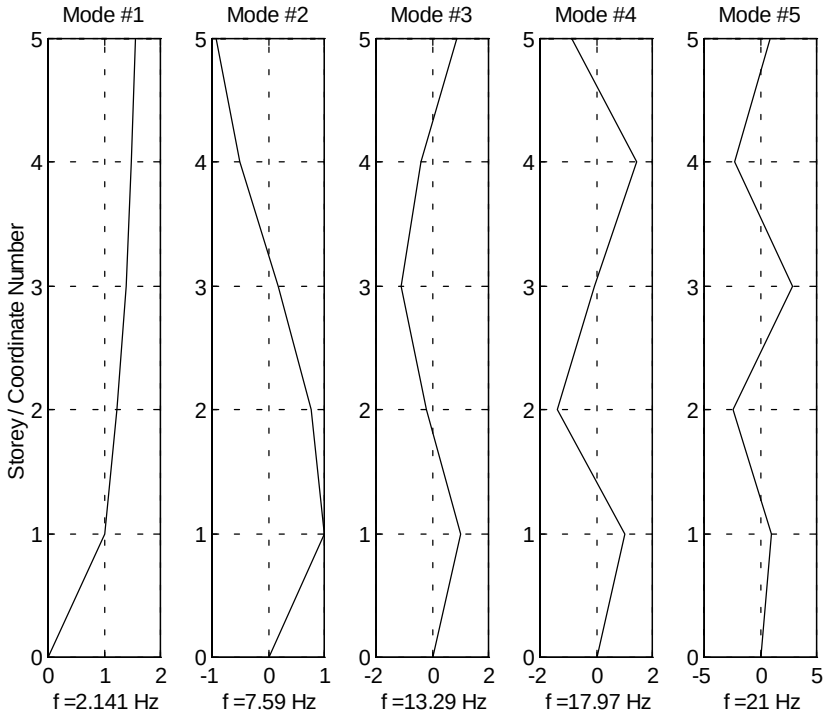

Figure 8.1: Magnitudes of the normalized complex mode shapes.

Storey No.	1. mode Magnitude	2. mode Magnitude	3. mode Magnitude	4. mode Magnitude	5. mode Magnitude
5	1.55	0.94	0.89	0.88	0.88
4	1.49	0.50	0.41	1.46	2.30
3	1.38	0.19	1.11	0.09	2.88
2	1.21	0.78	0.21	1.41	2.38
1	1	1	1	1	1

Table 8.2: Magnitudes of normalized complex mode shapes.

Storey No.	1. mode Phase [°]	2. mode Phase [°]	3. mode Phase [°]	4. mode Phase [°]	5. mode Phase [°]
5	-0.96	-179.72	1.88	-177.01	4.55
4	-0.58	-176.91	176.67	-0.33	-178.02
3	-0.46	-8.01	-179.43	154.89	2.26
2	-0.16	-0.83	-170.98	-179.28	-179.32
1	0	0	0	0	0

Table 8.3: Phase angels of normalized complex mode shapes.

Since all the modes are well separated and since the phase angles are close to 0° and $\pm 180^\circ$, the structural modes are close to being normal.

8.2 Simulating the System Response

This section describes how the system response is simulated and how disturbance is added. It is also explained how the ambient excitation of the plane frame structure is modelled and how to obtain a simulation model.

8.2.1 Discrete-Time Modelling and Addition of Disturbance

The process noise $\boldsymbol{w}(t_k)$ is assumed to be zero, and four different levels of the measurement noise $\boldsymbol{v}(t_k)$ are applied. The covariance matrix of the measurement noise is calculated as

$$\boldsymbol{R} = K\left(\frac{1}{p} \sum_{i=1}^{p} \sqrt{\boldsymbol{\Sigma}_{ii}(0)} \right)^2 \boldsymbol{I} \qquad \textbf{(4)}$$

where p is the number of output channels, and $\boldsymbol{\Sigma}_{ii}(0)$ correponds to the ith diagonal element of the sampled zero-lag covariance matrix of the noise-free output. K is a constant that controls the noise level and can be considered as a signal-to-noise ratio. In table 8.3 the values of K used in the analysis are listed.

No.	1	2	3	4
K	0.001	0.01	0.05	0.1

Table 8.3: The values of K to be used.

As seen the noise covariance matrix is defined as a diagonal matrix of the mean-square of the sampled standard deviations of the noise-free output multiplied by the signal-to-noise ratio K.

To avoid numerical integration of the structural system (8.1), which could be accomplished by a Runge-Kutta integration scheme, the continuous-time system is converted to a covariance equivalent discrete-time ARMAV(2,1) model. This conversion is performed using the technique described in theorem 4.2 in section 4.2.1. The sampling interval is $T = 0.02$ sec. The results of the conversion are two auto-regressive coefficient matrices together with one of 252 solutions of the moving average coefficient matrix and the associated covariance matrix of the zero-mean Gaussian white noise input process.

The auto-regressive coefficient matrices are given by

$$\boldsymbol{A}_1 = \begin{bmatrix} -0.620 & -1.073 & -0.253 & -0.016 & -0.002 \\ -1.137 & 0.284 & -0.925 & -0.213 & -0.022 \\ -0.242 & -0.889 & 0.269 & -0.889 & -0.237 \\ -0.022 & -0.214 & -0.920 & 0.282 & -1.071 \\ -0.001 & -0.020 & -0.236 & -1.070 & -0.293 \end{bmatrix} \quad \textbf{(5)}$$

$$\boldsymbol{A}_2 = \begin{bmatrix} 0.892 & 0.079 & -0.011 & 0.004 & -0.001 \\ 0.036 & 0.941 & 0.030 & 0.007 & -0.001 \\ -0.001 & 0.056 & 0.884 & 0.056 & -0.002 \\ -0.001 & 0.005 & 0.033 & 0.933 & 0.044 \\ 0 & 0.001 & 0 & 0.046 & 0.962 \end{bmatrix} \quad \textbf{(6)}$$

The moving average coefficient matrix is given by

$$\boldsymbol{B}_2 = \begin{bmatrix} 0.365 & -0.138 & 0.080 & -0.061 & 0.026 \\ -0.194 & 0.712 & -0.426 & 0.278 & -0.112 \\ 0.111 & -0.367 & 0.782 & -0.379 & 0.130 \\ -0.097 & 0.272 & -0.430 & 0.724 & -0.209 \\ 0.038 & -0.104 & 0.142 & -0.204 & 0.415 \end{bmatrix} \quad \textbf{(7)}$$

and its corresponding Gaussian white noise covariance matrix is given by

$$\boldsymbol{\Delta} = 10^{-5} \times \begin{bmatrix} 0.322 & 0.131 & 0.023 & 0.007 & -0.001 \\ 0.131 & 0.229 & 0.120 & 0.009 & 0.009 \\ 0.023 & 0.120 & 0.215 & 0.121 & 0.019 \\ 0.007 & 0.009 & 0.121 & 0.227 & 0.129 \\ -0.001 & 0.009 & 0.019 & 0.129 & 0.306 \end{bmatrix} \quad \textbf{(8)}$$

The noise can be incorporated into the system by using theorem 4.3 to yield a new ARMAV(2,2) model. However, since only measurement noise is added, it is easier to add the noise to the simulated noise-free output.

The final simulation model is obtained by conversion of the ARMAV(2,1) model to a state space realization using e.g. the techniques described in theorem 2.4 in section 2.5.1. The measurement noise is then added to yield

$$\begin{aligned} \boldsymbol{x}(t_{k+1}) &= \boldsymbol{A}\boldsymbol{x}(t_k) + \boldsymbol{B}\boldsymbol{u}(t_k) , \qquad \boldsymbol{u}(t_k) \in NID(\boldsymbol{0}, \boldsymbol{\Delta}) \\ \boldsymbol{y}(t_{k+1}) &= \boldsymbol{C}\boldsymbol{x}(t_k) + \boldsymbol{v}(t_k) , \qquad \boldsymbol{v}(t_k) \in NID(\boldsymbol{0}, \boldsymbol{R}) \end{aligned} \tag{9}$$

The response is then obtained by simulating the outcome of the p-variate Gaussian white noise processes $\boldsymbol{u}(t_k)$ and $\boldsymbol{v}(t_k)$, for $k = 1$ to N.

8.2.2 Organizing the Simulations

In addition to the use of four different values of the signal-to-noise parameter K four different record lengths N are used. This means that the number of simulation cases is 16. In each of these cases, 100 simulations and identifications have been performed. This implies that the total number of simulations and identifications is 1600.

The organization of the simulation study is shown in table 8.4.

	$K = 0.001$	$K = 0.01$	$K = 0.05$	$K = 0.1$
$N = 1250$	run11i	run12i	run13i	run14i
$N = 2500$	run21i	run22i	run23i	run24i
$N = 5000$	run31i	run32i	run33i	run34i
$N = 10000$	run41i	run42i	run43i	run44i

Table 8.4: Organization of the simulations. The integer i takes values between 1 and 100.

The simulations and identifications are performed using the STDI toolbox, described in section 7.3. The conversion from the continuous-time differential eqaution system to the ARMAV(2,1) model is performed by the routine armav21.m. The noise-free simulated system output is calculated by the routine ddssim.m. And finally, the PEM identification of an adequate ARMAV model is performed by the routine armav.m. This routine implements the robustified Gauss-Newton search scheme for the PEM estimator. This Gauss-Newton search scheme is given in definition 5.1 in section 5.3.1, and the robustification procedure is described in section 7.1.4.

8.3 The Results of the Simulation Study

In this section, the results of the simulation study will be presented. Since the simulations are performed using an ARMAV(2,1) model and since Gaussian white noise has been added, an adequate model structure is an ARMAV(2,2) model according to section 4.3. In figure 8.2, this is verified by plotting the FPE criterion for different identified ARMAV models of the simulation case run441, see table 8.4.

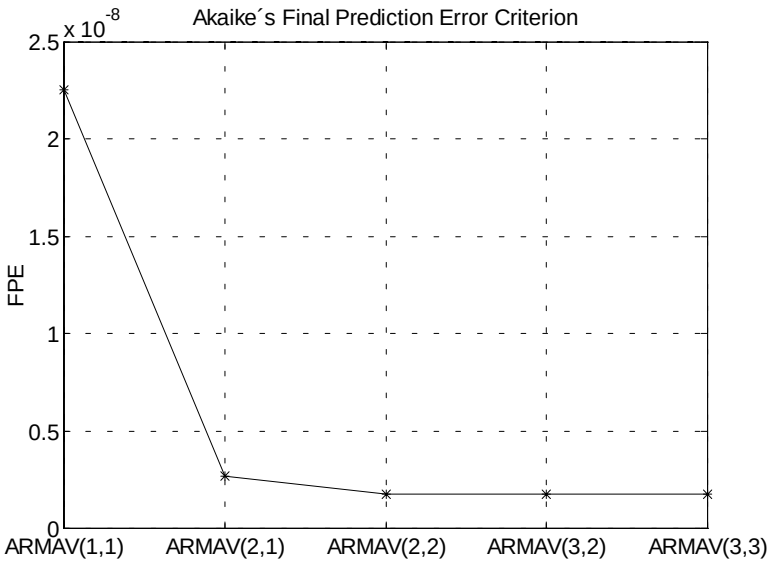

Figure 8.2: Akaike's FPE criterion plotted for the following choices of model structure. ARMAV(1,1), ARMAV(2,1), ARMAV(2,2), ARMAV(3,2) and ARMAV(3,3).

This model structure has been used in all 1600 simulations. In all cases the maximum number of iterations used in the PEM algorithm is 20. If this number is exceeded or if the RMS value of the search gradient, given by $\boldsymbol{R}_N^{-1}(\theta)\boldsymbol{F}_N(\theta)$ in definition 5.1, is less than 1.0×10^{-5} the iterations are stopped. The robustification parameter ρ that is used to remove outliers is set as 1.6, see section 7.1.4.

8.3.1 Adequacy of Chosen Number of Simulations

Besides checking the adequacy of the model structure, it is necessary to verify that the statistical properties of the estimates converge within the 100 simulations of each run. If it can be verified that the statistical properties converge in the worst case, then it will be assumed that the statistical properties in all the other cases also converge. The worst case is run14, since its record length is the shortest and the noise level is the highest.

The convergence check of the run14 simulations is performed by plotting the sampled standard deviation $\sigma_\kappa(m)$ of the modal parameter κ as a function of the number of simulations m. In other words, plotting the function

$$\sigma_\kappa(m) = \sqrt{\frac{1}{m}\sum_{k=1}^{m}\left(\hat{\kappa}(k) - \kappa_0\right)^2}\ , \qquad m = 2,\ 3,\ \ldots\ ,\ 100 \qquad \textbf{(10)}$$

The parameter κ_0 corresponds to the true modal parameter of the system being simulated. By using this parameter the sampled standard deviation will be unbiased. The modal parameter $\hat{\kappa}(k)$ is either the estimate of the kth simulation of one of the five natural eigenfrequencies, or one of the associated damping ratios, or one of the normalized mode shape coordinates of one of the five modes.

The change of the unbiased standard deviation defined in (8.10) of the five estimated natural eigenfrequencies of run14 is plotted in figure 8.3.

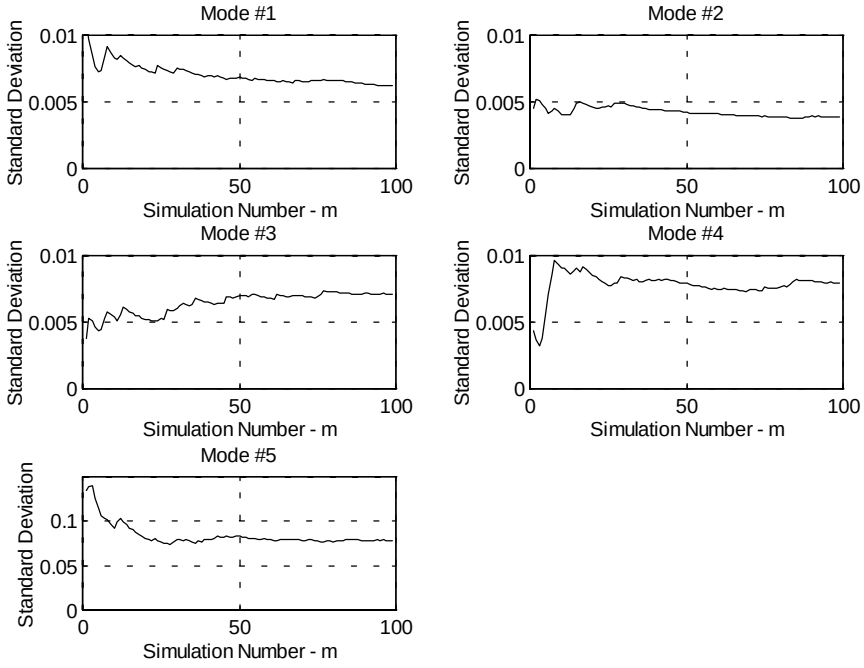

Figure 8.3: Change of the standard deviation of the five natural eigenfrequency estimates as a function of the number of simulations for run14.

After 50 simulations the changes of the standard deviations are beginning to saturate and at 100 simulations they have almost converged to constant values. It is therefore assumed that the chosen number of simulations with regard to the natural eigenfrequencies is adequate. The estimated damping ratios of the five modes will be analysed in a similar manner. The changes of the standard deviation of the five estimated damping ratios of run14 are plotted in figure 8.4.

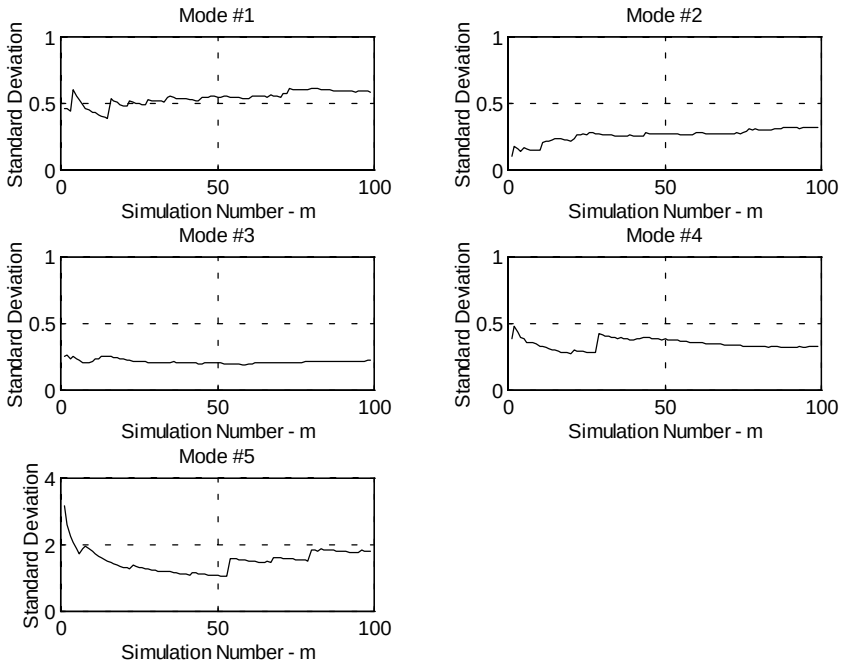

Figure 8.4: Changes of the standard deviation of the five damping ratio estimates as a function of the number of simulations for run14.

Again, the standard deviations seem to converge to constant values, which implies that the chosen number of simulations with regard to the damping ratios is adequate.

The next five plots show the absolute change of the standard deviation of the scaled mode shapes of the five modes. Each of the mode shapes has been normalized with respect to their first coordinate. Due to this normalization this coordinate will always be one and therefore have the standard deviation zero.

In figures 8.5 to 8.9, the changes of the standard deviation of the remaining mode shape coordinates are plotted for each of the five modes.

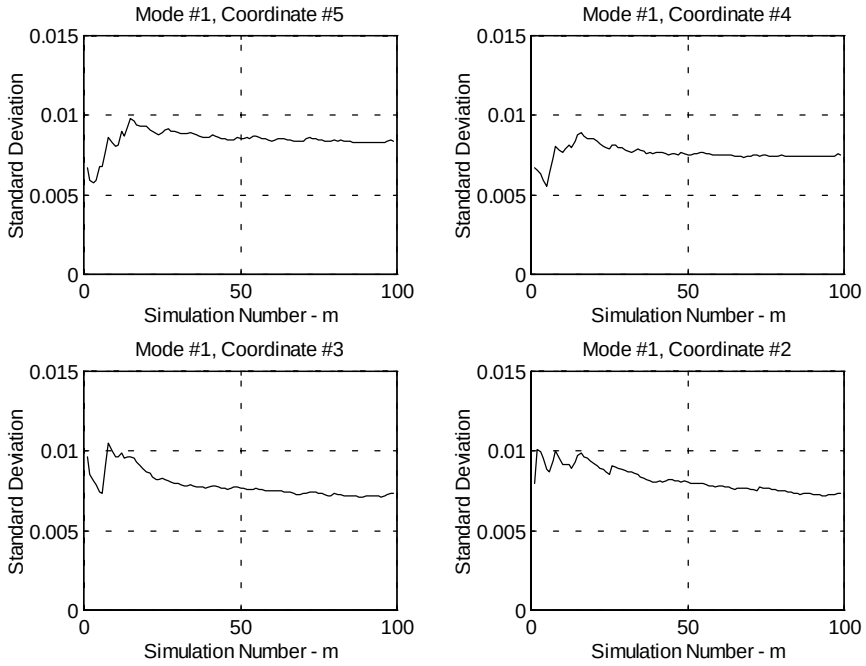

Figure 8.5: Changes of the standard deviation of the four mode shape coordinate estimates of the first mode as a function of the number of simulations for run14.

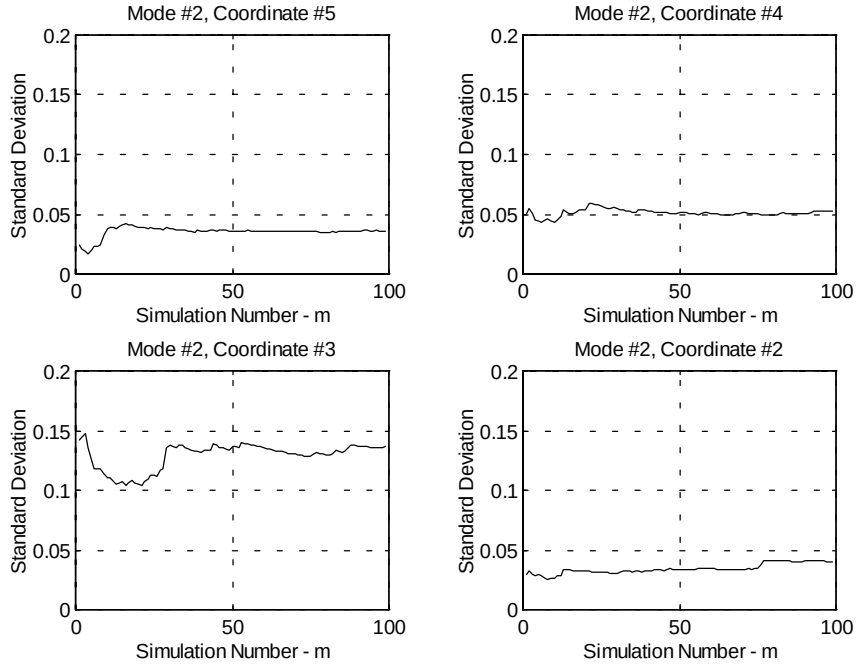

Figure 8.6: Changes of the standard deviation of the four mode shape coordinate estimates of the second mode as a function of the number of simulations for run14.

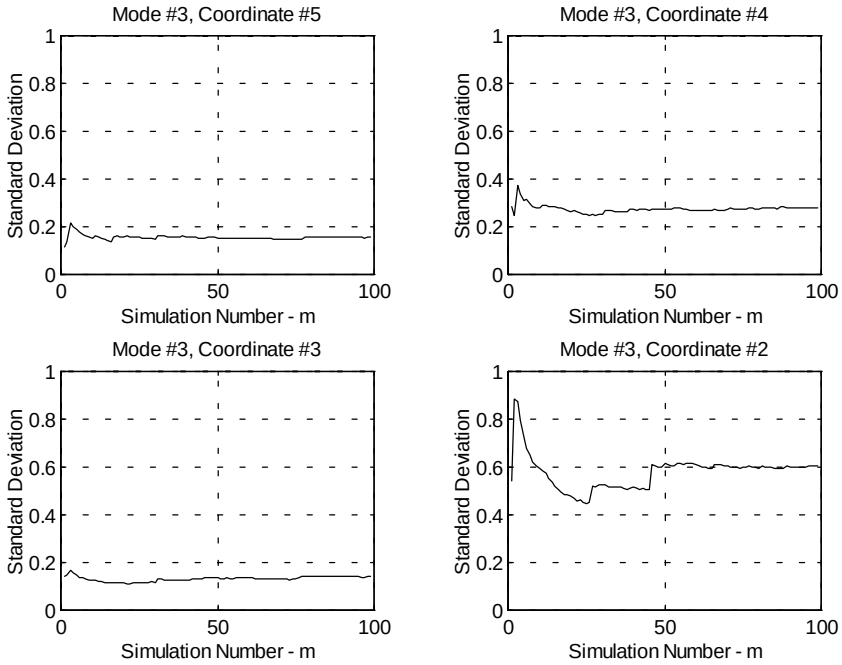

Figure 8.7: Changes of the standard deviation of the four mode shape coordinate estimates of the third mode as a function of the number of simulations for run14.

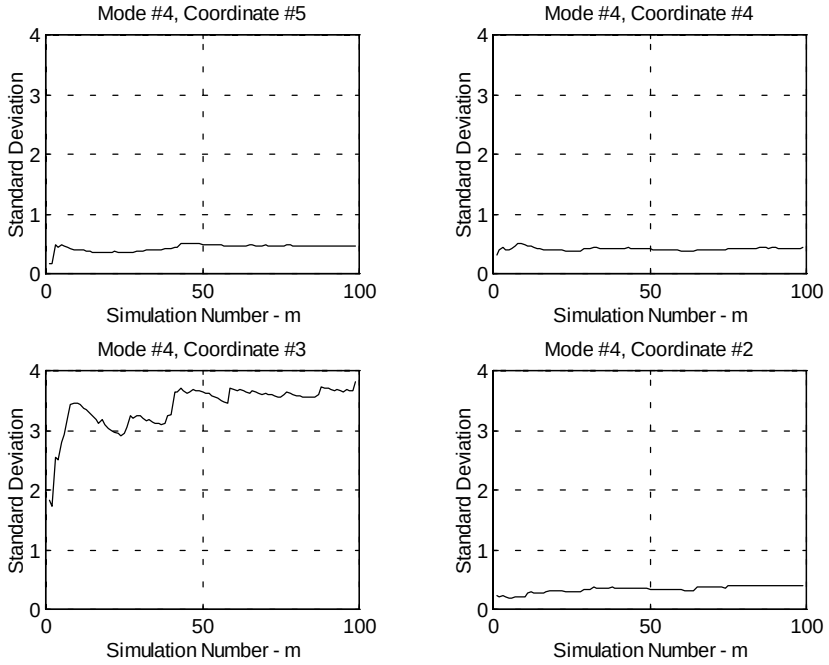

Figure 8.8: Changes of the standard deviation of the four mode shape coordinate estimates of the fourth mode as a function of the number of simulations for run14.

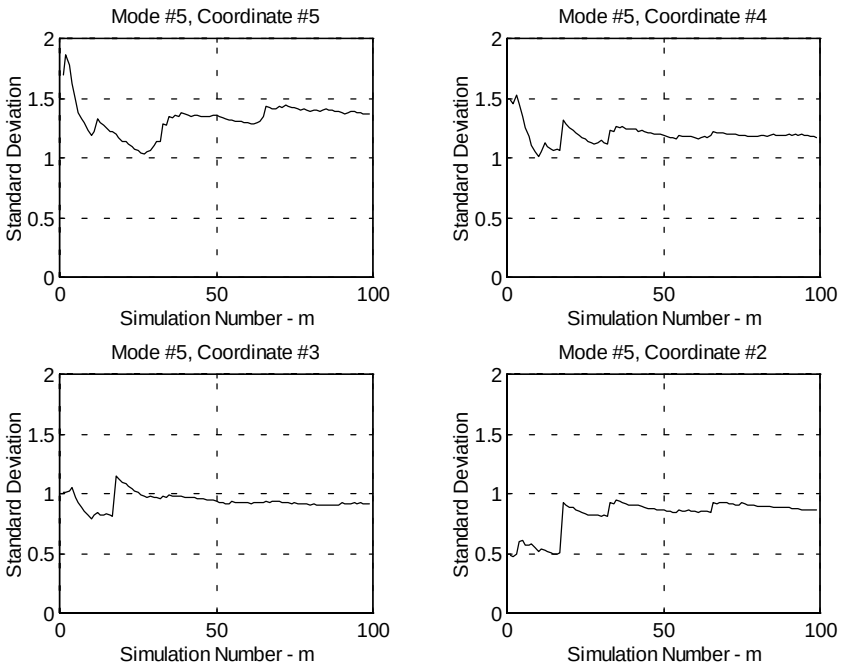

Figure 8.9: Changes of the standard deviation of the four mode shape coordinate estimates of the fifth mode as a function of the number of simulations for run14.

The standard deviations of the mode shape coordinates also seem to converge to constant values in all cases.

So in conclusion :

☞ *In case of run14, which is assumed to be the worst of the 16 cases presented in table 8.4, it has been shown that 100 simulations are enough to obtain convergent statistical properties of the estimated modal parameters. On the basis of this observation, it is therefore assumed that 100 simulation will also be enough in all the other cases.*

In the following the number of simulations *m* will therefore be a constant parameter, defined as $m = 100$.

8.3.2 Bias of Estimated Modal Parameters

In section 5.5.2, it was stated that the estimated model parameters will be asymptotically unbiased if the true system is contained in the model structure and if the prediction errors are Gaussian white noise. Due to the analytical relation between the model and modal parameters these requirements also result in asymptotically unbiased modal parameters.

Therefore, to be able to say that the estimated modal parameters are asymptotically unbiased, the following remains to be verified :

- ☞ *Adequacy of the model structure.*
- ☞ *Prediction errors are Gaussian white noise.*

At the beginning of this section, it was verified that the applied ARMAV(2,2) model was adequate, which means that the true system can be assumed contained in the model. Since the excitation and the applied noise in all the simulations are Gaussian distributed realizations, verification remains that the prediction errors of the identified models are white noise realizations.

Since the unbiasness is an asymptotical property of the PEM estimator the following analysis is performed for the simulation case run41, which has the maximum record length. To prove whether the prediction errors are white noise or not, estimates of the autocorrelation function can be plotted. The estimated autocorrelation function for a white noise process should be approximately zero except at the zero lag. Further, since the realizations of the excitation and the applied noise originate from the same stochastic excitation and noise processes, any numerical inaccuracies can be reduced by averaging of the estimated autocovariance of the prediction errors obtained from each of the 100 simulations.

In figure 8.10 the averaged autocorrelation functions of the five channels obtained from run41 are plotted.

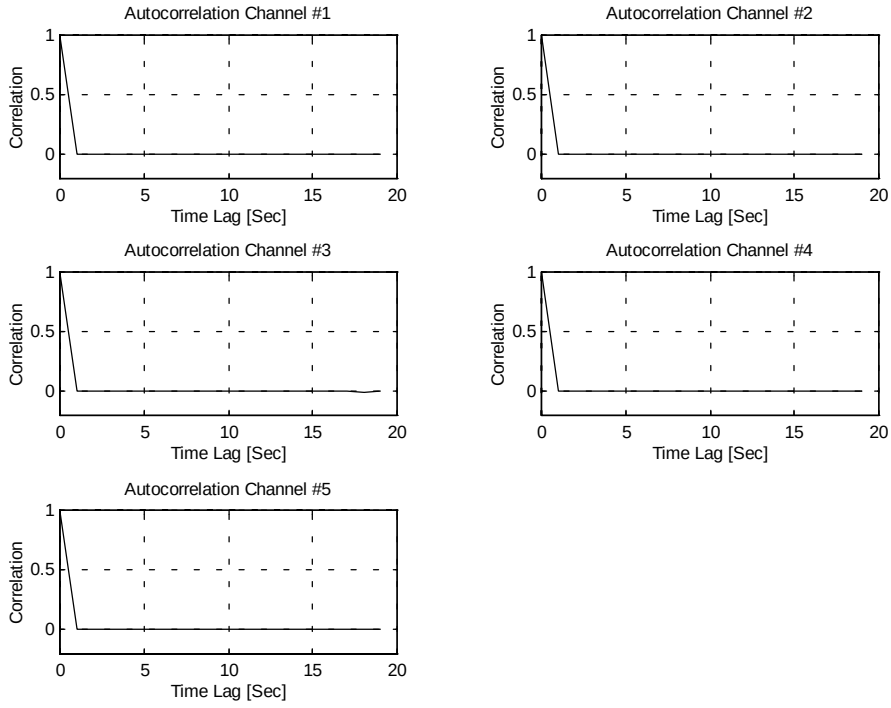

Figure 8.10: Averaged autocorrelation functions of run41.

The autocorrelation at the non-zero time-lags are seen to be close to zero. This implies that the prediction errors forms a realization of a multivariate white noise process.

So in conclusion :

☞ *The above analysis indicates that if the true system is contained in the model, it is possible to obtain prediction errors that are white noise.*

To visualize how the bias changes as a function of *N* and *K* the following bias measures are plotted for all 16 simulation cases.

$$\beta_\kappa = \frac{1}{m}\sum_{k=1}^{m}\frac{\hat{\kappa}(k) - \kappa_0}{\kappa_0}, \qquad \begin{cases} \kappa = f_i \ \ for \ i = 1,\ 2,\ \ldots,\ 5 \\ \kappa = \zeta_i \ \ for \ i = 1,\ 2,\ \ldots,\ 5 \end{cases}$$

$$\beta_\kappa = \left| \frac{1}{m}\sum_{k=1}^{m}\hat{\kappa}(k) - \kappa_0 \right|, \qquad \kappa = \Phi_{ij} \ for \begin{cases} i = 1,\ 2,\ \ldots,\ 5 \\ j = 2,\ \ldots,\ 5 \end{cases} \qquad \textbf{(11)}$$

The first bias measure is applied for the natural eigenfrequency and the associated damping ratio, whereas the last bias measure is applied for each of the mode shape coordinates Φ_{ij} where *i* indicate the mode and *j* the coordinate number according to figure 8.1.

In figures 8.11 to 8.13 the first bias measure of (8.11) is plotted as a function of the record length *N* and the noise level *K*.

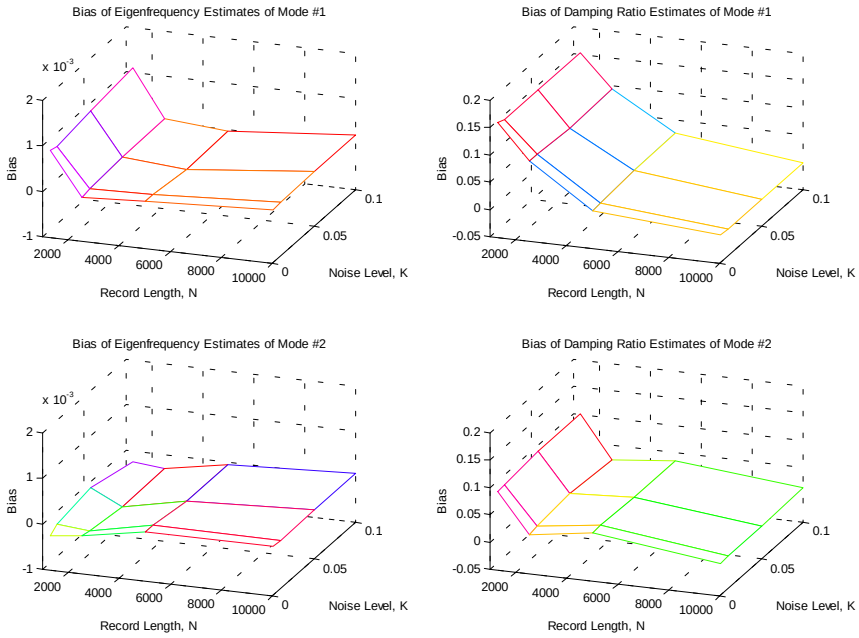

Figure 8.11: Estimated bias of the first and second natural eigenfrequencies and associated damping ratios as a function of record length *N* and noise level *K*.

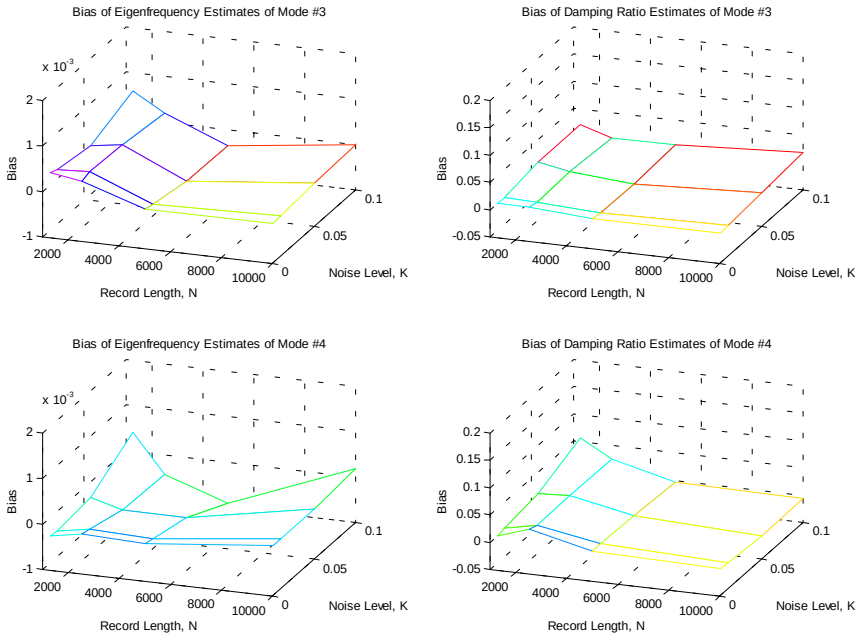

Figure 8.12: Estimated bias of the third and fourth natural eigenfrequencies and associated damping ratios as a function of record length *N* and noise level *K*.

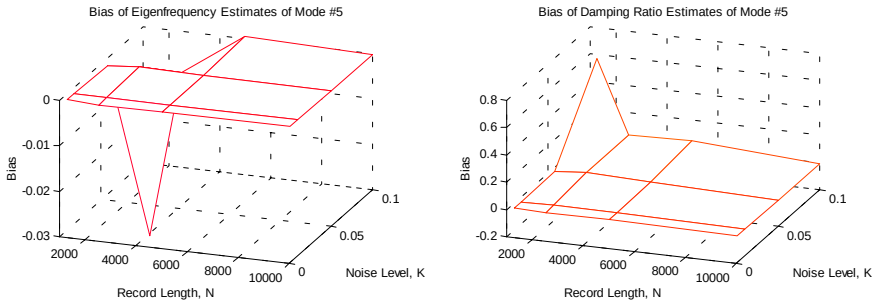

Figure 8.13: Estimated bias of the fifth natural eigenfrequency and associated damping ratio as a function of record length *N* and noise level *K*.

In figures 8.14 to 8.18 the bias of each of the mode shapes is plotted coordinate-wise as a function of the record length and the noise level.

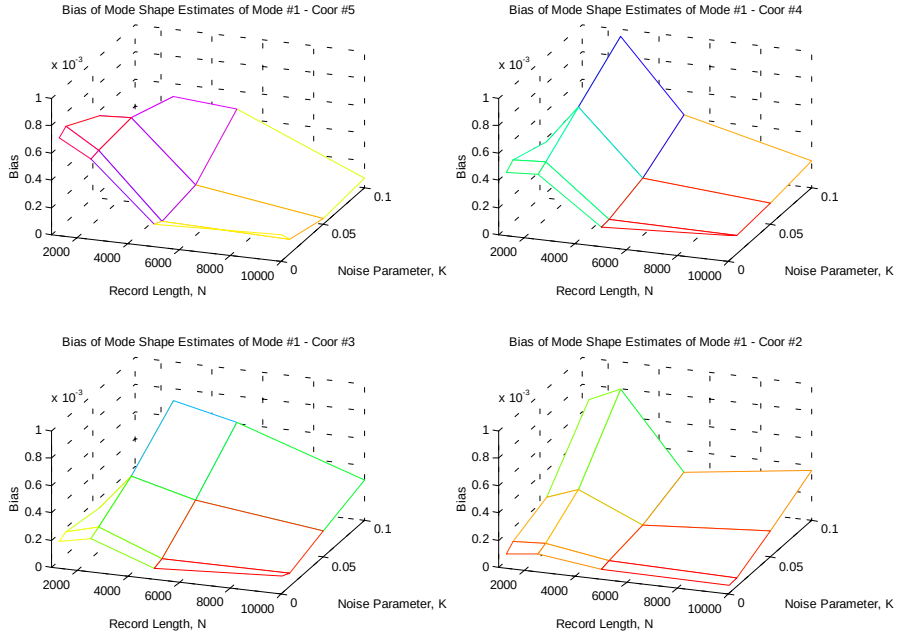

Figure 8.14: Estimated bias of the mode shape coordinates of the first mode as a function of record length *N* and noise level *K*.

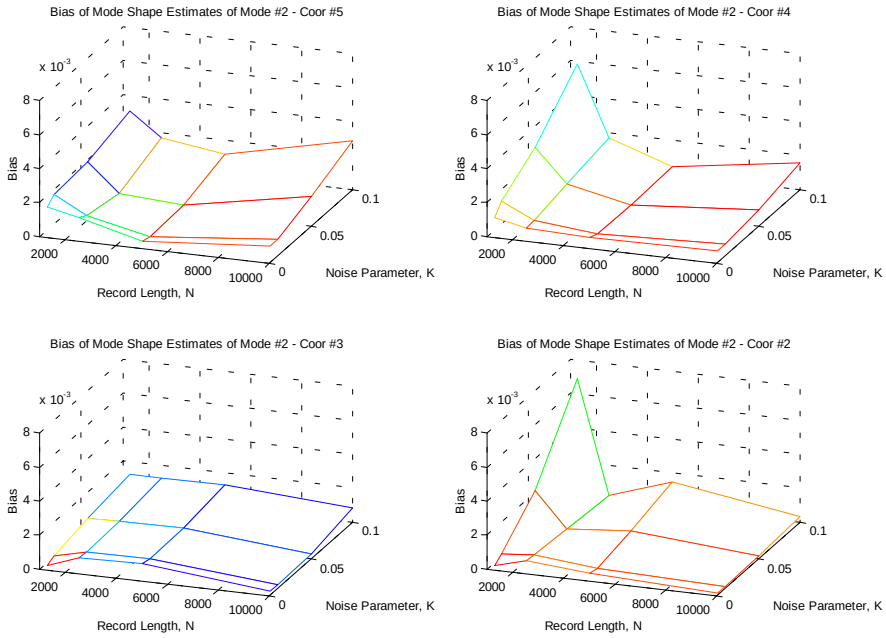

Figure 8.15: Estimated bias of the mode shape coordinates of the second mode as a function of record length *N* and noise level *K*.

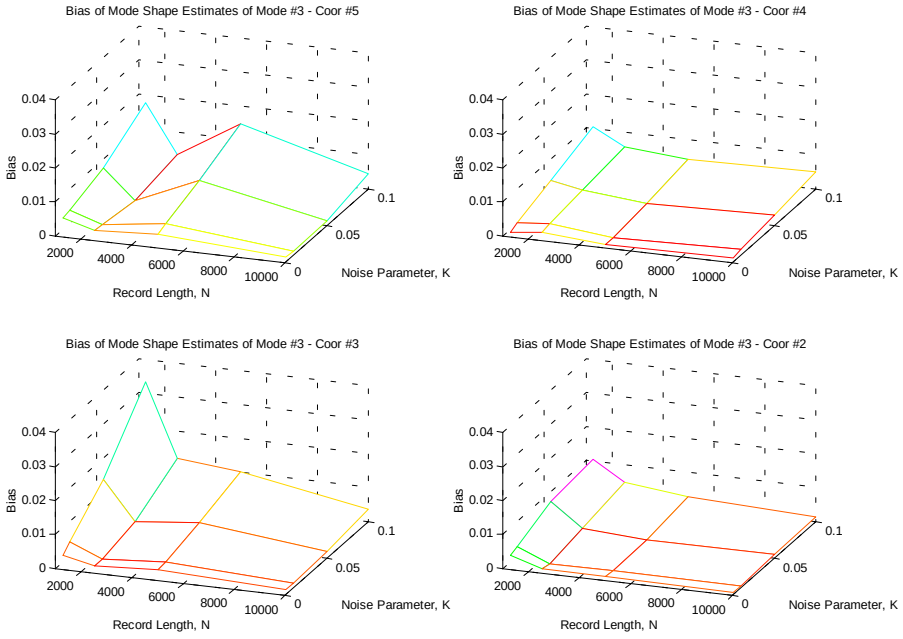

Figure 8.16: Estimated bias of the mode shape coordinates of the third mode as a function of record length *N* and noise level *K*.

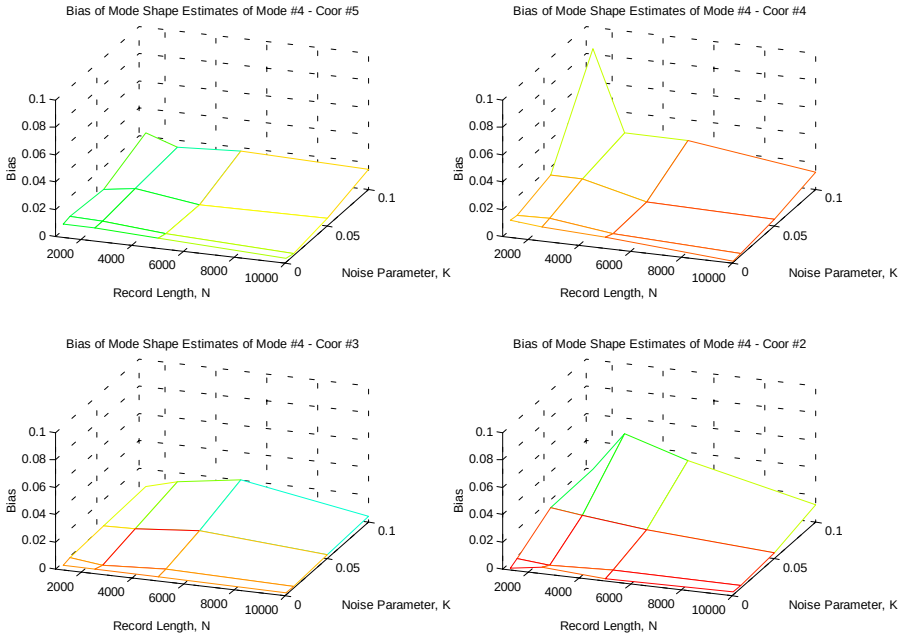

Figure 8.17: Estimated bias of the mode shape coordinates of the fourth mode as a function of record length *N* and noise level *K*.

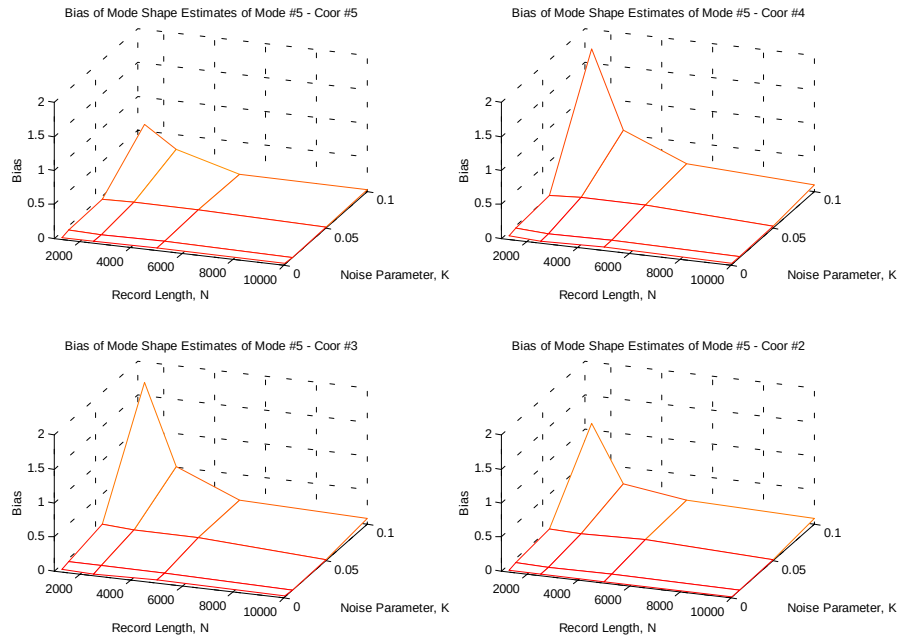

Figure 8.18: Estimated bias of the mode shape coordinates of the fifth mode as a function of record length *N* and noise level *K*.

All figures presented in this section indicate that the bias increases rapidly as the number of samples decreases. When the record length exceeds $N = 5000$ the decrease of the bias of the natural eigenfrequencies and the damping ratios begin to saturate for all levels of noise. However, the bias of the mode shapes is still descreasing at the high noise levels. In general, the bias of the mode shapes is seen to be more dependent on the presence of noise than on the record length as seen in figures 8.16, 8.17 and 8.18. This is in contrast to the bias of the natural eigenfrequencies and the damping ratios, which in general is more dependent on the record length than on the noise level as seen in figures 8.11 and 8.12.

In most of the cases, it is seen that the bias keeps descreasing as the number of samples is increased. This indicates that the estimator in the present simulation study will be asymptotically unbiased.

8.3.3 Sampled and Estimated Standard Deviations

In section 6.2, it was explained how the standard deviation of the estimated modal parameters could be estimated on the basis of the approximative Hessian matrix. This matrix could be obtained directly from a PEM algorithm that implements the Gauss-Newton search procedure. In this section a comparison between the standard deviations of the modal parameters obtained using this approach and the sampled standard deviations will be made.

Since the true mean values κ_0 of the modal parameters are known in advance, the following unbiased sampled coefficient of variation ν_k has been applied in the comparison.

$$\nu_\kappa = \frac{\sqrt{\frac{1}{m}\sum_{k=1}^{m}\left(\hat{\kappa}(k) - \kappa_0\right)^2}}{\kappa_0} \qquad \textbf{(12)}$$

This coefficient of variation is preferred instead of the standard deviation itself. This is because it is non-dimensional and as such makes comparison of the different modal parameters easier. In the case of the mode shapes ν_k is complex. In this case the magnitude of ν_k is used.

In each of the 16 simulation cases 100 simulations were performed. This implies that the standard deviation of each of the modal parameters has been estimated 100 times. To make use of all simulations these 100 estimates have been averaged in the following analysis. These averaged standard deviations are also divided by the true mean values in order to obtain the coefficient of variation. These estimated coefficients of variation are denoted $\hat{\nu}_\kappa$ to distinguish these from the sampled coefficients of variation ν_k.

In the following figures 8.19 to 8.33 the sampled and estimated coefficients of variation ν_k and $\hat{\nu}_\kappa$ of the estimated natural eigenfrequencies, damping ratios and mode shape coordinates of the five modes will be presented. The left-hand sub-plots will be the sampled coefficients of variation ν_k defined in (8.12), whereas the right-hand sub-plots will be the coefficients of variation $\hat{\nu}_\kappa$ estimated from the Hessian matrix.

Below each of the figures the normalized differences $|\nu_k - \hat{\nu}_\kappa|/\nu_k$ between the sampled and estimated coefficients of variations of the 16 simulation cases will be listed in tables.

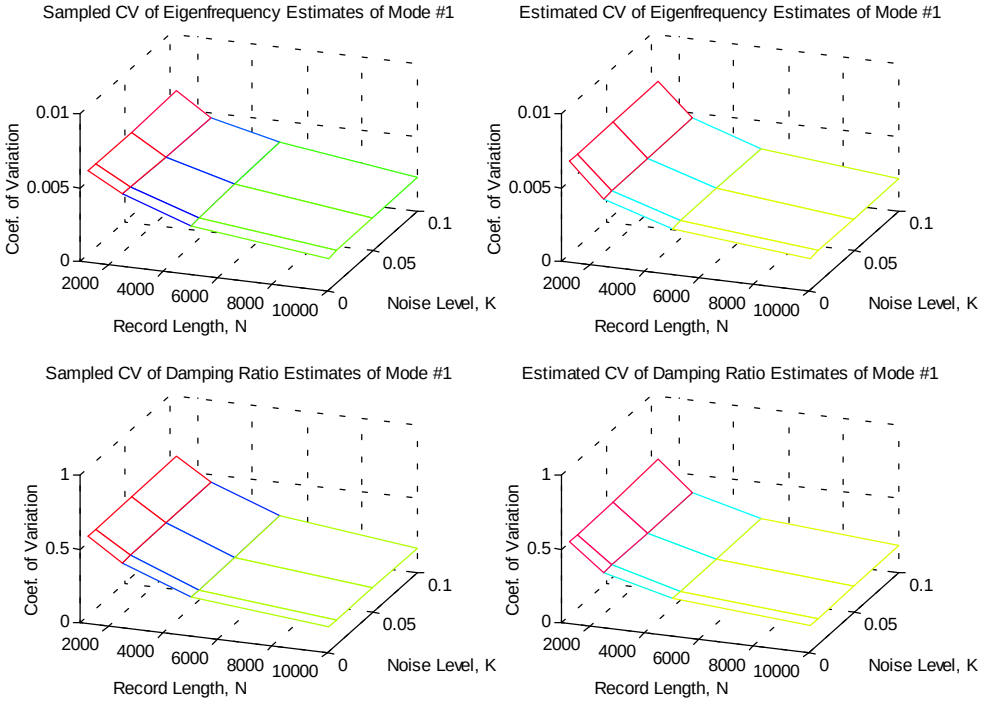

Figure 8.19: Sampled and estimated coefficients of variation for the estimates of the natural eigenfrequency and associated damping ratios of the first mode.

	$K = 0.001$	$K = 0.01$	$K = 0.05$	$K = 0.1$
$N = 1250$	-1.0×10^{-1}	-9.6×10^{-2}	-1.2×10^{-1}	-1.1×10^{-1}
$N = 2500$	6.8×10^{-2}	5.3×10^{-2}	2.4×10^{-2}	1.1×10^{-2}
$N = 5000$	4.7×10^{-2}	5.8×10^{-2}	8.9×10^{-2}	1.1×10^{-1}
$N = 10000$	8.6×10^{-3}	2.4×10^{-2}	2.9×10^{-2}	2.2×10^{-2}

Table 8.5: Normalized differences of sampled and estimated coefficients of variation of estimated natural eigenfrequencies of the first mode.

	$K = 0.001$	$K = 0.01$	$K = 0.05$	$K = 0.1$
$N = 1250$	6.7×10^{-2}	6.5×10^{-2}	6.2×10^{-2}	3.1×10^{-2}
$N = 2500$	1.4×10^{-1}	1.5×10^{-1}	1.5×10^{-1}	1.5×10^{-1}
$N = 5000$	3.6×10^{-2}	2.8×10^{-2}	3.9×10^{-2}	7.6×10^{-2}
$N = 10000$	-4.9×10^{-2}	-4.6×10^{-2}	-6.9×10^{-2}	-6.4×10^{-2}

Table 8.6: Normalized differences of sampled and estimated coefficients of variation of estimated damping ratios of the first mode.

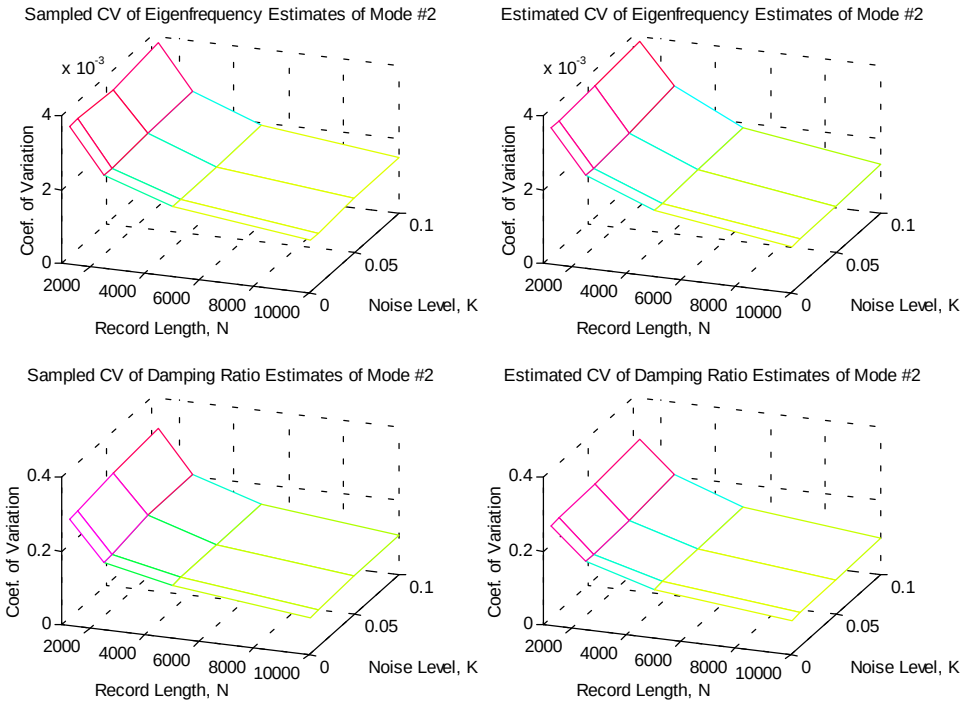

Figure 8.20: Sampled and estimated coefficients of variation for the estimates of the natural eigenfrequency and associated damping ratios of the second mode.

	$K = 0.001$	$K = 0.01$	$K = 0.05$	$K = 0.1$
$N = 1250$	1.3×10^{-2}	1.4×10^{-2}	-3.1×10^{-2}	-1.5×10^{-2}
$N = 2500$	-3.0×10^{-3}	-2.0×10^{-4}	9.6×10^{-3}	-5.5×10^{-2}
$N = 5000$	5.3×10^{-2}	4.8×10^{-2}	4.3×10^{-2}	3.0×10^{-2}
$N = 10000$	1.3×10^{-1}	1.2×10^{-1}	1.4×10^{-1}	1.2×10^{-1}

Table 8.7: Normalized differences of sampled and estimated coefficients of variation of estimated natural eigenfrequencies of the second mode.

	$K = 0.001$	$K = 0.01$	$K = 0.05$	$K = 0.1$
$N = 1250$	5.5×10^{-2}	6.3×10^{-2}	9.6×10^{-2}	9.3×10^{-2}
$N = 2500$	-8.7×10^{-3}	-1.0×10^{-2}	6.2×10^{-2}	-1.4×10^{-2}
$N = 5000$	8.3×10^{-2}	9.3×10^{-2}	8.0×10^{-2}	4.7×10^{-2}
$N = 10000$	5.9×10^{-2}	7.6×10^{-2}	9.3×10^{-2}	8.8×10^{-2}

Table 8.8: Normalized differences of sampled and estimated coefficients of variation of estimated damping ratios of the second mode.

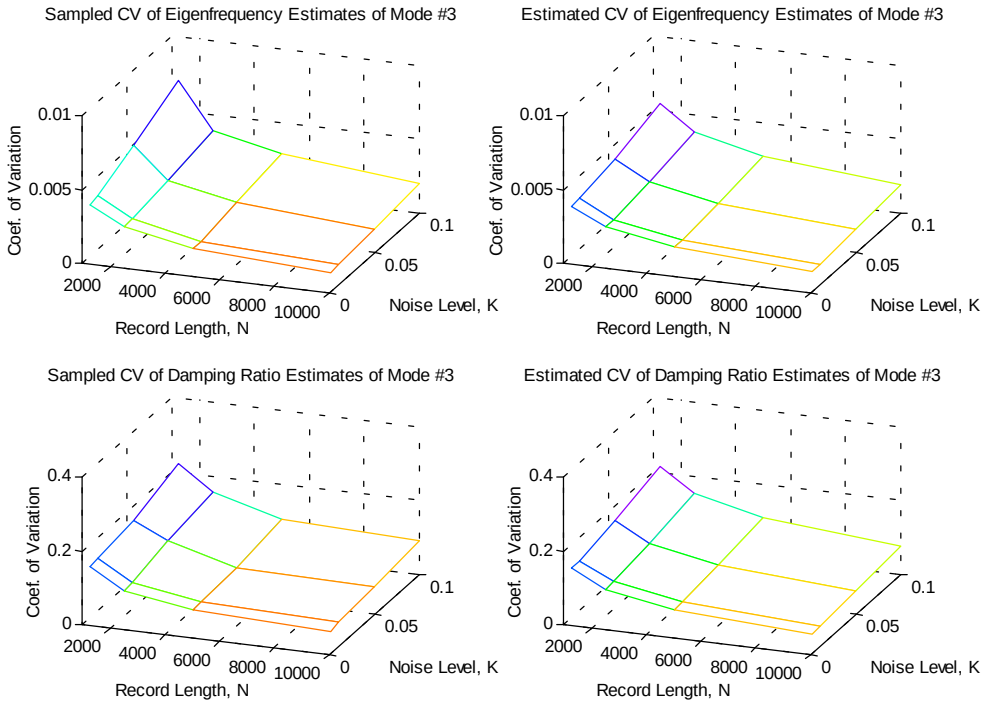

Figure 8.21: Sampled and estimated coefficients of variation for the estimates of the natural eigenfrequency and associated damping ratios of the third mode.

	$K = 0.001$	$K = 0.01$	$K = 0.05$	$K = 0.1$
$N = 1250$	2.9×10^{-2}	4.5×10^{-2}	1.6×10^{-1}	2.3×10^{-1}
$N = 2500$	9.0×10^{-3}	3.0×10^{-2}	3.2×10^{-2}	2.7×10^{-2}
$N = 5000$	-2.9×10^{-2}	-4.1×10^{-2}	4.0×10^{-2}	7.5×10^{-2}
$N = 10000$	-3.0×10^{-3}	-6.8×10^{-3}	-1.2×10^{-2}	7.0×10^{-3}

Table 8.9: Normalized differences of sampled and estimated coefficients of variation of estimated natural eigenfrequencies of the third mode.

	$K = 0.001$	$K = 0.01$	$K = 0.05$	$K = 0.1$
$N = 1250$	4.1×10^{-2}	3.1×10^{-2}	-1.1×10^{-2}	2.9×10^{-2}
$N = 2500$	-2.6×10^{-2}	-3.4×10^{-2}	5.3×10^{-2}	3.1×10^{-2}
$N = 5000$	-9.6×10^{-3}	-5.0×10^{-4}	-7.3×10^{-2}	-4.6×10^{-2}
$N = 10000$	1.2×10^{-1}	1.5×10^{-1}	1.4×10^{-1}	1.5×10^{-1}

Table 8.10: Normalized differences of sampled and estimated coefficients of variation of estimated damping ratios of the third mode.

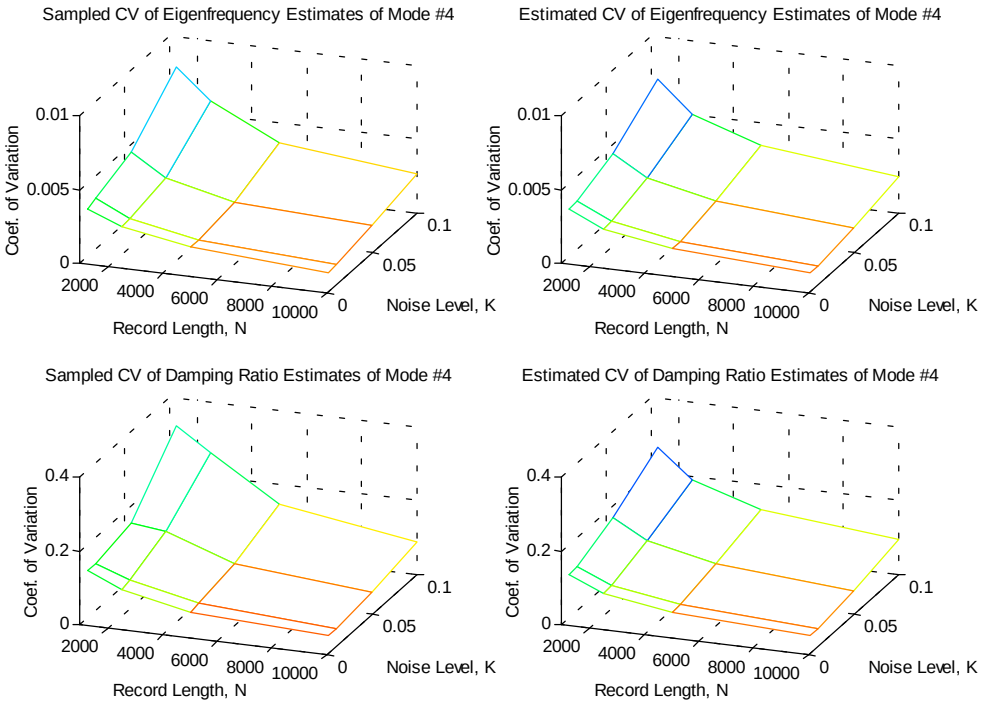

Figure 8.22: Sampled and estimated coefficients of variation for the estimates of the natural eigenfrequency and associated damping ratios of the fourth mode.

	$K = 0.001$	$K = 0.01$	$K = 0.05$	$K = 0.1$
$N = 1250$	9.0×10^{-3}	5.4×10^{-2}	1.1×10^{-2}	1.1×10^{-1}
$N = 2500$	3.8×10^{-2}	4.6×10^{-2}	-1.3×10^{-2}	1.6×10^{-1}
$N = 5000$	6.7×10^{-2}	3.2×10^{-2}	-3.3×10^{-2}	5.7×10^{-2}
$N = 10000$	2.5×10^{-2}	4.1×10^{-2}	7.6×10^{-2}	9.4×10^{-2}

Table 8.11: Normalized differences of sampled and estimated coefficients of variation of estimated natural eigenfrequencies of the fourth mode.

	$K = 0.001$	$K = 0.01$	$K = 0.05$	$K = 0.1$
$N = 1250$	7.1×10^{-2}	3.2×10^{-2}	-7.2×10^{-2}	1.8×10^{-1}
$N = 2500$	9.8×10^{-2}	1.2×10^{-1}	1.7×10^{-1}	2.8×10^{-1}
$N = 5000$	-1.1×10^{-3}	2.7×10^{-2}	2.4×10^{-2}	8.9×10^{-2}
$N = 10000$	-3.5×10^{-3}	1.5×10^{-3}	-8.3×10^{-2}	-6.7×10^{-2}

Table 8.12: Normalized differences of sampled and estimated coefficients of variation of estimated damping ratios of the fourth mode.

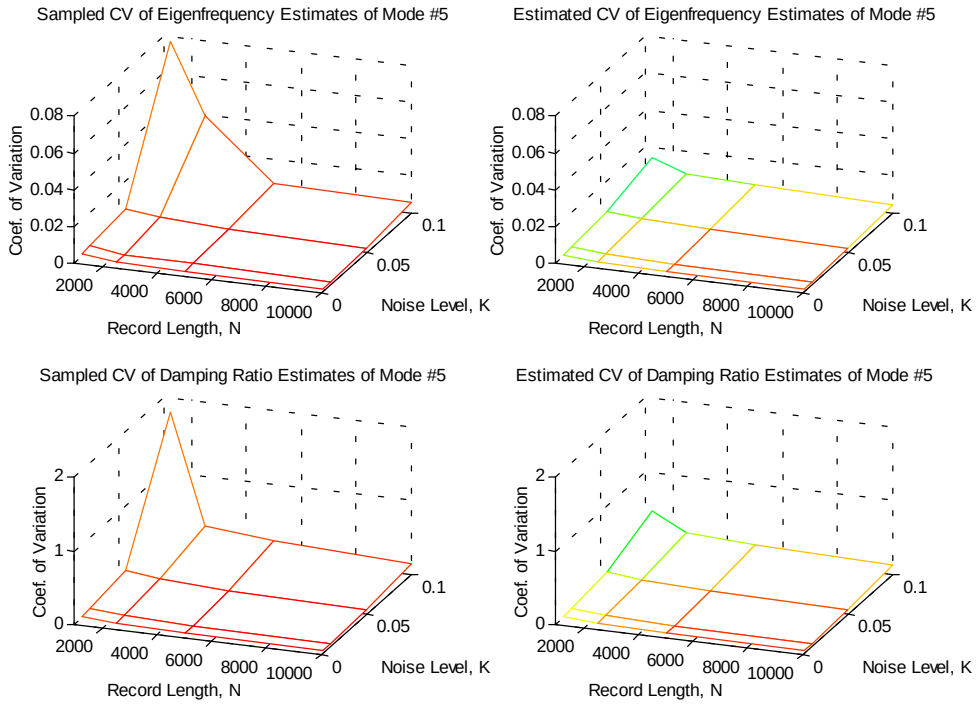

Figure 8.23: Sampled and estimated coefficients of variation for the estimates of the natural eigenfrequency and associated damping ratios of the fifth mode.

	$K = 0.001$	$K = 0.01$	$K = 0.05$	$K = 0.1$
$N = 1250$	5.9×10^{-2}	1.1×10^{-1}	1.6×10^{-1}	8.1×10^{-1}
$N = 2500$	-5.5×10^{-2}	-5.2×10^{-2}	1.3×10^{-1}	8.0×10^{-1}
$N = 5000$	9.8×10^{-2}	1.2×10^{-1}	1.3×10^{-1}	1.5×10^{-1}
$N = 10000$	5.2×10^{-2}	3.4×10^{-2}	9.2×10^{-2}	2.2×10^{-1}

Table 8.13: Normalized differences of sampled and estimated coefficients of variation of estimated natural eigenfrequencies of the fifth mode.

	$K = 0.001$	$K = 0.01$	$K = 0.05$	$K = 0.1$
$N = 1250$	4.3×10^{-2}	4.2×10^{-2}	6.7×10^{-2}	7.3×10^{-1}
$N = 2500$	1.6×10^{-2}	4.0×10^{-2}	7.1×10^{-2}	2.6×10^{-1}
$N = 5000$	1.4×10^{-2}	-1.2×10^{-3}	5.6×10^{-2}	2.0×10^{-1}
$N = 10000$	2.4×10^{-3}	-2.0×10^{-2}	5.5×10^{-2}	7.8×10^{-2}

Table 8.14: Normalized differences of sampled and estimated coefficients of variation of estimated damping ratios of the fifth mode.

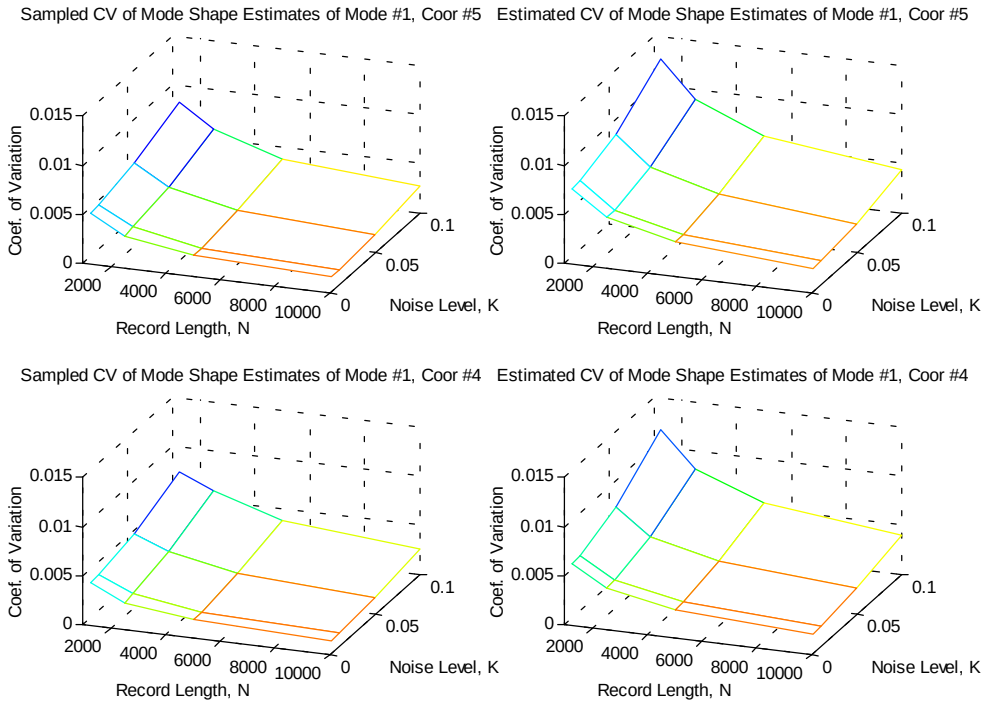

Figure 8.24: Sampled and estimated coefficients of variation for the estimates of the mode shape coordinates 5 and 4 of the first mode.

	$K = 0.001$	$K = 0.01$	$K = 0.05$	$K = 0.1$
$N = 1250$	-4.6×10^{-1}	-4.6×10^{-1}	-4.8×10^{-1}	-5.2×10^{-1}
$N = 2500$	-5.6×10^{-1}	-5.2×10^{-1}	-4.7×10^{-1}	-5.0×10^{-1}
$N = 5000$	-6.5×10^{-1}	-6.5×10^{-1}	-6.2×10^{-1}	-6.2×10^{-1}
$N = 10000$	-5.6×10^{-1}	-5.7×10^{-1}	-5.9×10^{-1}	-6.0×10^{-1}

Table 8.15: Normalized differences of sampled and estimated coefficients of the variation of estimated mode shape coordinate 5 of the first mode.

	$K = 0.001$	$K = 0.01$	$K = 0.05$	$K = 0.1$
$N = 1250$	-4.3×10^{-1}	-4.4×10^{-1}	-4.9×10^{-1}	-5.6×10^{-1}
$N = 2500$	-5.3×10^{-1}	-4.7×10^{-1}	-3.7×10^{-1}	-3.8×10^{-1}
$N = 5000$	-5.5×10^{-1}	-5.6×10^{-1}	-5.0×10^{-1}	-4.7×10^{-1}
$N = 10000$	-4.9×10^{-1}	-5.0×10^{-1}	-5.5×10^{-1}	-5.7×10^{-1}

Table 8.16: Normalized differences of sampled and estimated coefficients of the variation of estimated mode shape coordinate 4 of the first mode.

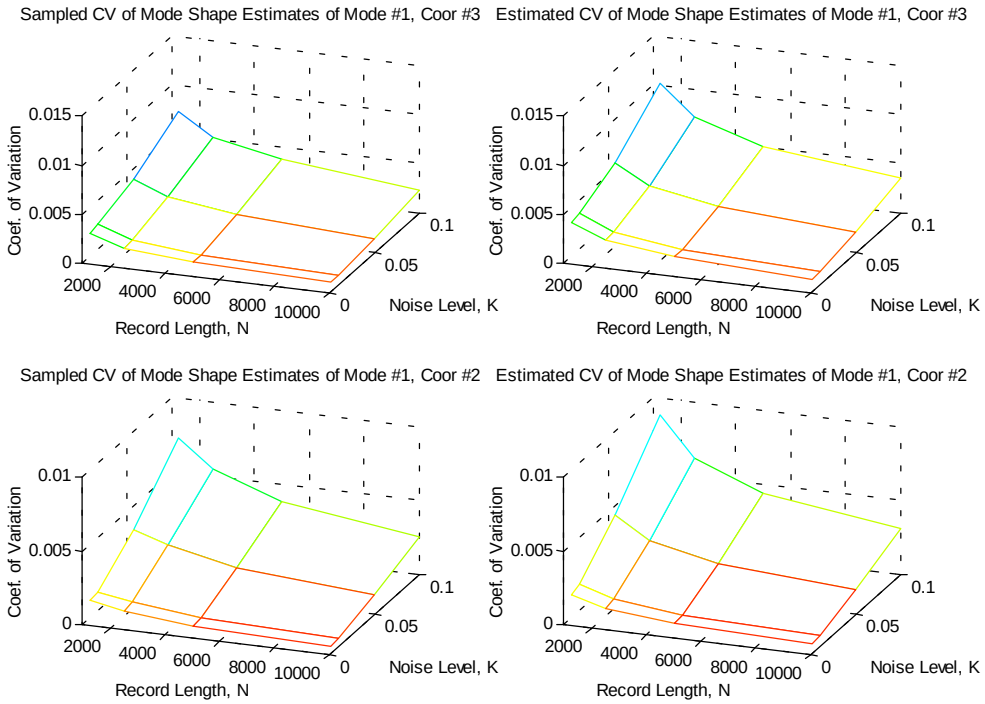

Figure 8.25: Sampled and estimated coefficients of variation for the estimates of the mode shape coordinates 3 and 2 of the first mode.

	$K = 0.001$	$K = 0.01$	$K = 0.05$	$K = 0.1$
$N = 1250$	-3.5×10^{-1}	-3.3×10^{-1}	-3.6×10^{-1}	-4.0×10^{-1}
$N = 2500$	-4.0×10^{-1}	-3.7×10^{-1}	-3.7×10^{-1}	-3.8×10^{-1}
$N = 5000$	-4.0×10^{-1}	-3.9×10^{-1}	-3.2×10^{-1}	-3.1×10^{-1}
$N = 10000$	-3.8×10^{-1}	-4.0×10^{-1}	-5.2×10^{-1}	-5.4×10^{-1}

Table 8.17: Normalized differences of sampled and estimated coefficients of the variation of estimated mode shape coordinate 3 of the first mode.

	$K = 0.001$	$K = 0.01$	$K = 0.05$	$K = 0.1$
$N = 1250$	-2.4×10^{-1}	-2.6×10^{-1}	-2.5×10^{-1}	-2.1×10^{-1}
$N = 2500$	-1.6×10^{-1}	-1.0×10^{-1}	-1.0×10^{-1}	-1.4×10^{-1}
$N = 5000$	-2.5×10^{-1}	-2.1×10^{-1}	-1.5×10^{-1}	-1.4×10^{-1}
$N = 10000$	-2.3×10^{-1}	-2.4×10^{-1}	-2.6×10^{-1}	-2.3×10^{-1}

Table 8.18: Normalized differences of sampled and estimated coefficients of the variation of estimated mode shape coordinate 2 of the first mode.

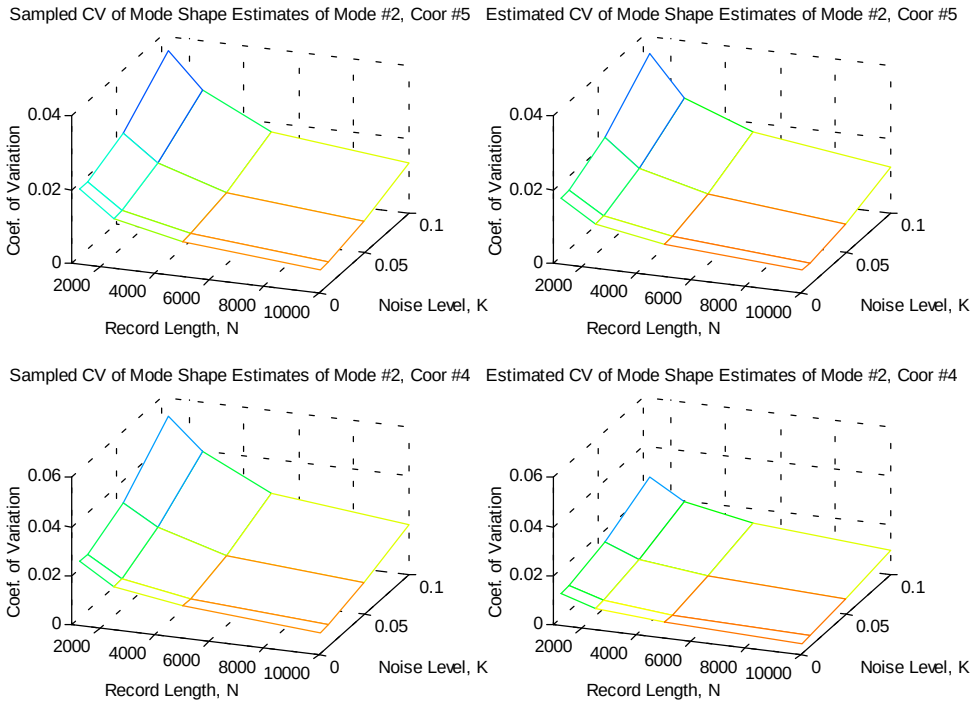

Figure 8.26: Sampled and estimated coefficients of variation for the estimates of the mode shape coordinates 5 and 4 of the second mode.

	$K = 0.001$	$K = 0.01$	$K = 0.05$	$K = 0.1$
$N = 1250$	1.2×10^{-1}	1.1×10^{-1}	5.3×10^{-2}	1.9×10^{-2}
$N = 2500$	8.9×10^{-2}	9.0×10^{-2}	9.5×10^{-2}	7.7×10^{-2}
$N = 5000$	8.2×10^{-2}	7.6×10^{-2}	2.6×10^{-2}	-4.0×10^{-4}
$N = 10000$	2.8×10^{-2}	3.9×10^{-2}	7.1×10^{-2}	9.3×10^{-2}

Table 8.19: Normalized differences of sampled and estimated coefficients of the variation of estimated mode shape coordinate 5 of the second mode.

	$K = 0.001$	$K = 0.01$	$K = 0.05$	$K = 0.1$
$N = 1250$	5.1×10^{-1}	4.9×10^{-1}	4.7×10^{-1}	4.7×10^{-1}
$N = 2500$	5.0×10^{-1}	5.0×10^{-1}	5.1×10^{-1}	5.1×10^{-1}
$N = 5000$	5.2×10^{-1}	5.1×10^{-1}	4.9×10^{-1}	4.7×10^{-1}
$N = 10000$	5.0×10^{-1}	5.0×10^{-1}	5.2×10^{-1}	5.1×10^{-1}

Table 8.20: Normalized differences of sampled and estimated coefficients of the variation of estimated mode shape coordinate 4 of the second mode.

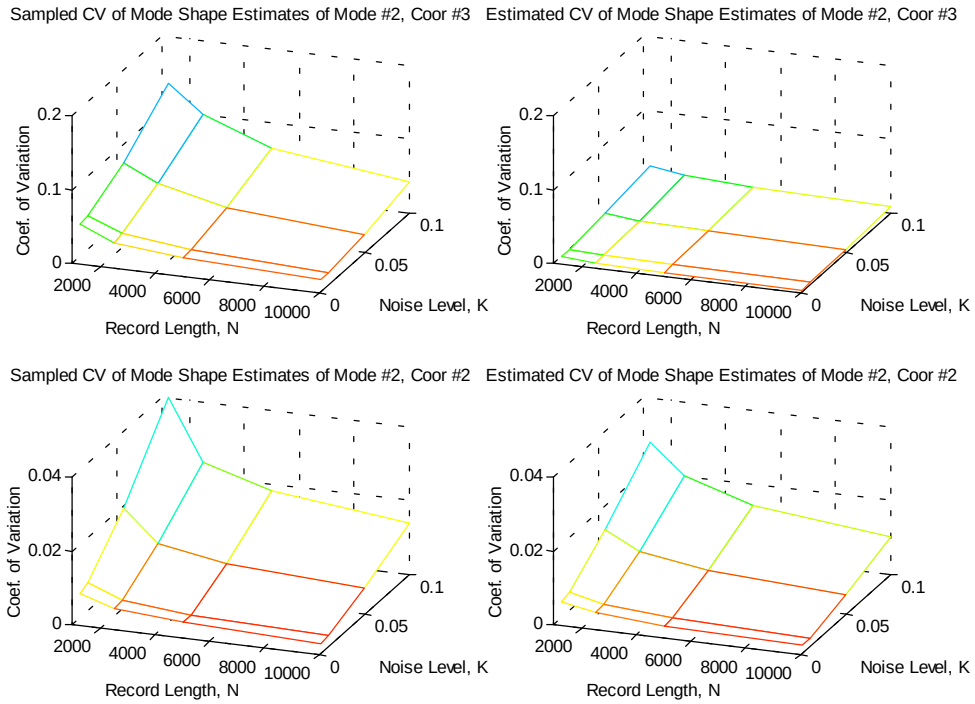

Figure 8.27: Sampled and estimated coefficients of variation for the estimates of the mode shape coordinates 3 and 2 of the second mode.

	$K = 0.001$	$K = 0.01$	$K = 0.05$	$K = 0.1$
$N = 1250$	8.2×10^{-1}	8.2×10^{-1}	8.2×10^{-1}	8.2×10^{-1}
$N = 2500$	8.1×10^{-1}	8.1×10^{-1}	8.3×10^{-1}	8.3×10^{-1}
$N = 5000$	8.2×10^{-1}	8.1×10^{-1}	8.1×10^{-1}	8.1×10^{-1}
$N = 10000$	8.1×10^{-1}	8.0×10^{-1}	7.9×10^{-1}	8.0×10^{-1}

Table 8.21: Normalized differences of sampled and estimated coefficients of the variation of estimated mode shape coordinate 3 of the second mode.

	$K = 0.001$	$K = 0.01$	$K = 0.05$	$K = 0.1$
$N = 1250$	2.5×10^{-1}	2.6×10^{-1}	2.8×10^{-1}	3.0×10^{-1}
$N = 2500$	2.0×10^{-1}	1.7×10^{-1}	1.7×10^{-1}	1.6×10^{-1}
$N = 5000$	2.2×10^{-1}	1.8×10^{-1}	2.0×10^{-1}	2.1×10^{-1}
$N = 10000$	2.3×10^{-1}	2.3×10^{-1}	2.7×10^{-1}	2.7×10^{-1}

Table 8.22: Normalized differences of sampled and estimated coefficients of the variation of estimated mode shape coordinate 2 of the second mode.

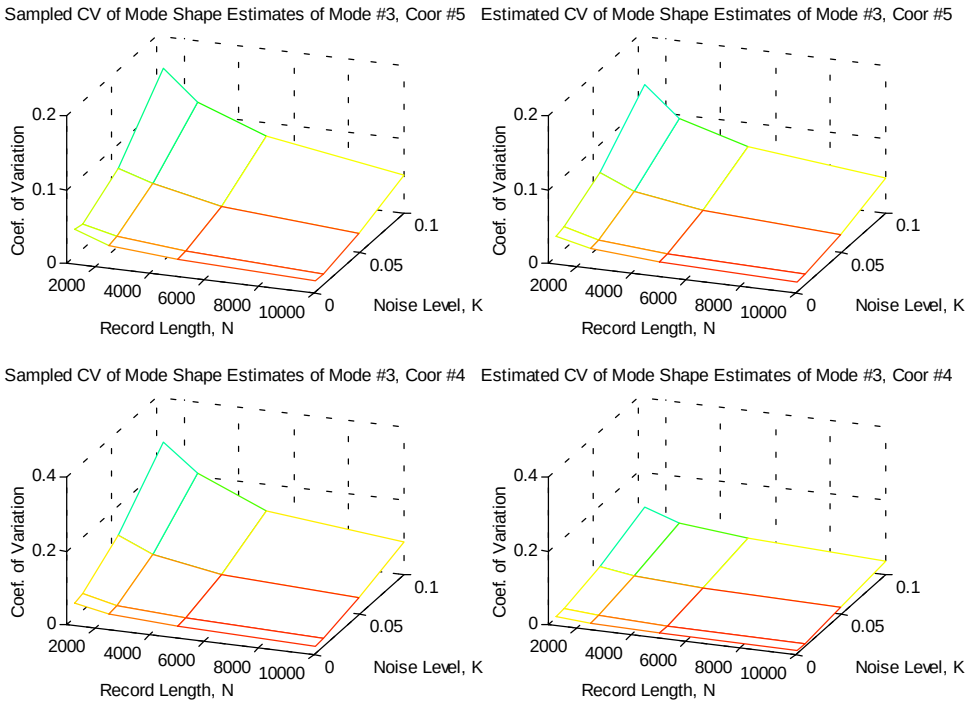

Figure 8.28: Sampled and estimated coefficients of variation for the estimates of the mode shape coordinates 5 and 4 of the third mode.

	$K = 0.001$	$K = 0.01$	$K = 0.05$	$K = 0.1$
$N = 1250$	1.7×10^{-1}	1.2×10^{-1}	7.9×10^{-2}	1.5×10^{-1}
$N = 2500$	1.4×10^{-1}	1.4×10^{-1}	1.9×10^{-1}	1.9×10^{-1}
$N = 5000$	1.8×10^{-1}	1.6×10^{-1}	1.3×10^{-1}	1.7×10^{-1}
$N = 10000$	1.5×10^{-1}	1.0×10^{-1}	2.3×10^{-2}	5.3×10^{-2}

Table 8.23: Normalized differences of sampled and estimated coefficients of the variation of estimated mode shape coordinate 5 of the third mode.

	$K = 0.001$	$K = 0.01$	$K = 0.05$	$K = 0.1$
$N = 1250$	6.0×10^{-1}	6.1×10^{-1}	6.2×10^{-1}	6.2×10^{-1}
$N = 2500$	6.2×10^{-1}	6.1×10^{-1}	6.2×10^{-1}	6.5×10^{-1}
$N = 5000$	6.2×10^{-1}	6.1×10^{-1}	5.7×10^{-1}	5.8×10^{-1}
$N = 10000$	6.1×10^{-1}	6.0×10^{-1}	5.7×10^{-1}	5.8×10^{-1}

Table 8.24: Normalized differences of sampled and estimated coefficients of the variation of estimated mode shape coordinate 4 of the third mode.

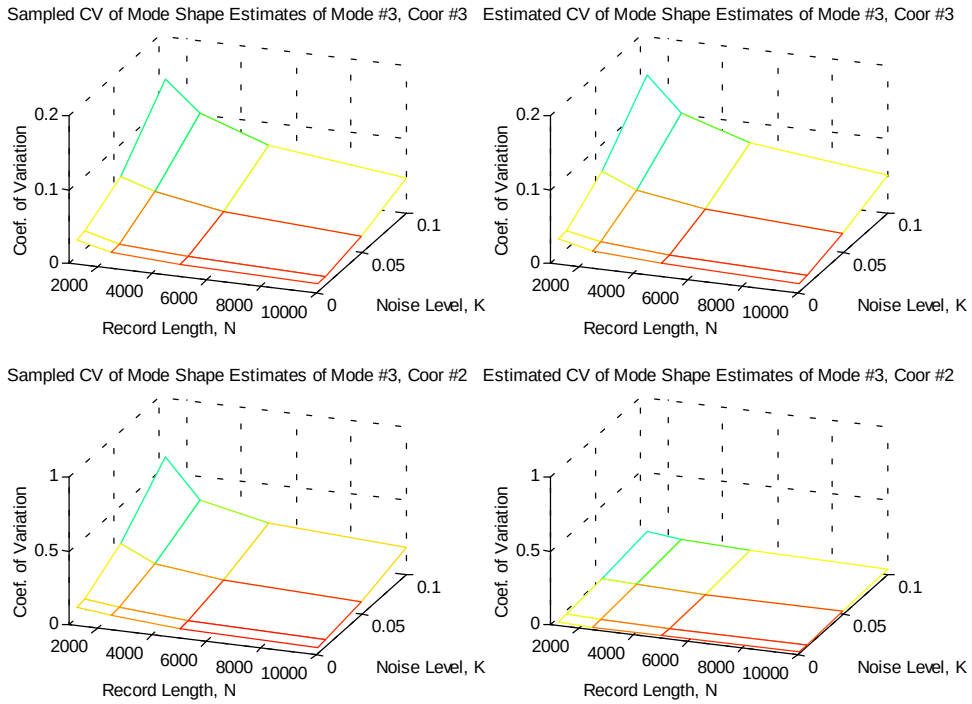

Figure 8.29: Sampled and estimated coefficients of variation for the estimates of the mode shape coordinates 3 and 2 of the third mode.

	$K = 0.001$	$K = 0.01$	$K = 0.05$	$K = 0.1$
$N = 1250$	-3.1×10^{-2}	-4.1×10^{-2}	-1.2×10^{-1}	-3.7×10^{-2}
$N = 2500$	-1.1×10^{-1}	-1.4×10^{-1}	-1.5×10^{-2}	-8.6×10^{-3}
$N = 5000$	-2.4×10^{-2}	-3.0×10^{-2}	-6.5×10^{-2}	-7.4×10^{-2}
$N = 10000$	-5.4×10^{-2}	-1.1×10^{-1}	-1.4×10^{-1}	-8.7×10^{-2}

Table 8.25: Normalized differences of sampled and estimated coefficients of the variation of estimated mode shape coordinate 3 of the third mode.

	$K = 0.001$	$K = 0.01$	$K = 0.05$	$K = 0.1$
$N = 1250$	8.0×10^{-1}	8.0×10^{-1}	8.2×10^{-1}	8.3×10^{-1}
$N = 2500$	8.2×10^{-1}	8.2×10^{-1}	8.0×10^{-1}	7.9×10^{-1}
$N = 5000$	7.8×10^{-1}	7.9×10^{-1}	7.8×10^{-1}	7.9×10^{-1}
$N = 10000$	7.8×10^{-1}	7.9×10^{-1}	8.0×10^{-1}	8.0×10^{-1}

Table 8.26: Normalized differences of sampled and estimated coefficients of the variation of estimated mode shape coordinate 2 of the third mode.

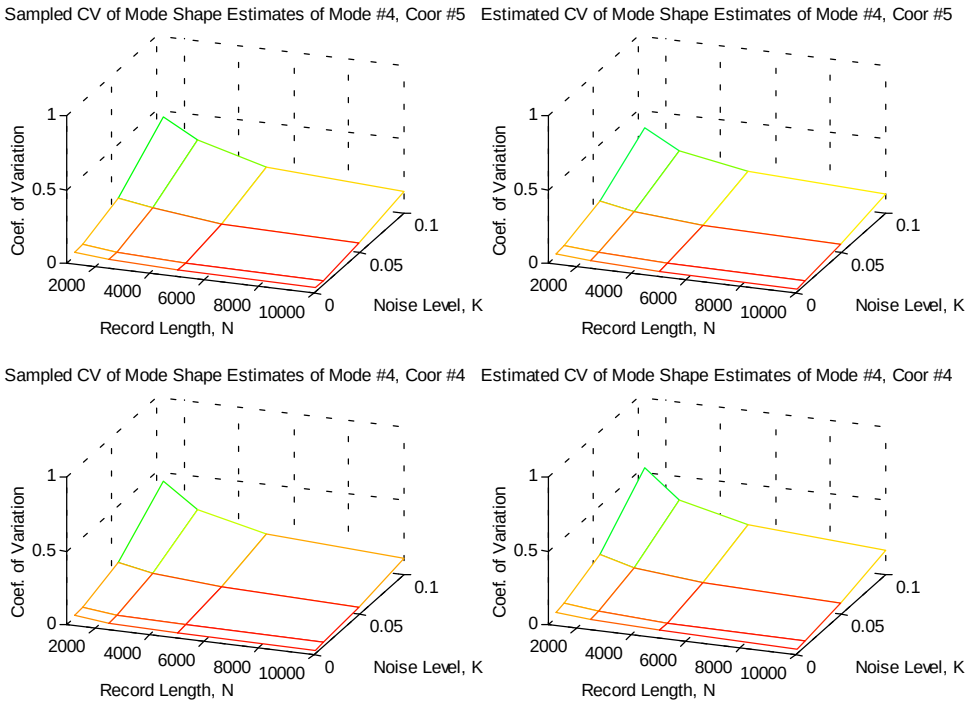

Figure 8.30: Sampled and estimated coefficients of variation for the estimates of the mode shape coordinates 5 and 4 of the fourth mode.

	$K = 0.001$	$K = 0.01$	$K = 0.05$	$K = 0.1$
$N = 1250$	1.6×10^{-1}	1.5×10^{-1}	1.2×10^{-1}	1.7×10^{-1}
$N = 2500$	1.6×10^{-1}	1.5×10^{-1}	1.7×10^{-1}	2.4×10^{-1}
$N = 5000$	1.7×10^{-1}	1.2×10^{-1}	9.9×10^{-2}	1.2×10^{-1}
$N = 10000$	1.6×10^{-1}	1.5×10^{-1}	1.4×10^{-1}	1.5×10^{-1}

Table 8.27: Normalized differences of sampled and estimated coefficients of the variation of estimated mode shape coordinate 5 of the fourth mode.

	$K = 0.001$	$K = 0.01$	$K = 0.05$	$K = 0.1$
$N = 1250$	-4.1×10^{-1}	-3.8×10^{-1}	-3.6×10^{-1}	-2.2×10^{-1}
$N = 2500$	-4.7×10^{-1}	-4.7×10^{-1}	-3.9×10^{-1}	-2.3×10^{-1}
$N = 5000$	-3.5×10^{-1}	-4.1×10^{-1}	-4.6×10^{-1}	-4.3×10^{-1}
$N = 10000$	-3.8×10^{-1}	-4.3×10^{-1}	-5.5×10^{-1}	-5.6×10^{-1}

Table 8.28: Normalized differences of sampled and estimated coefficients of the variation of estimated mode shape coordinate 4 of the fourth mode.

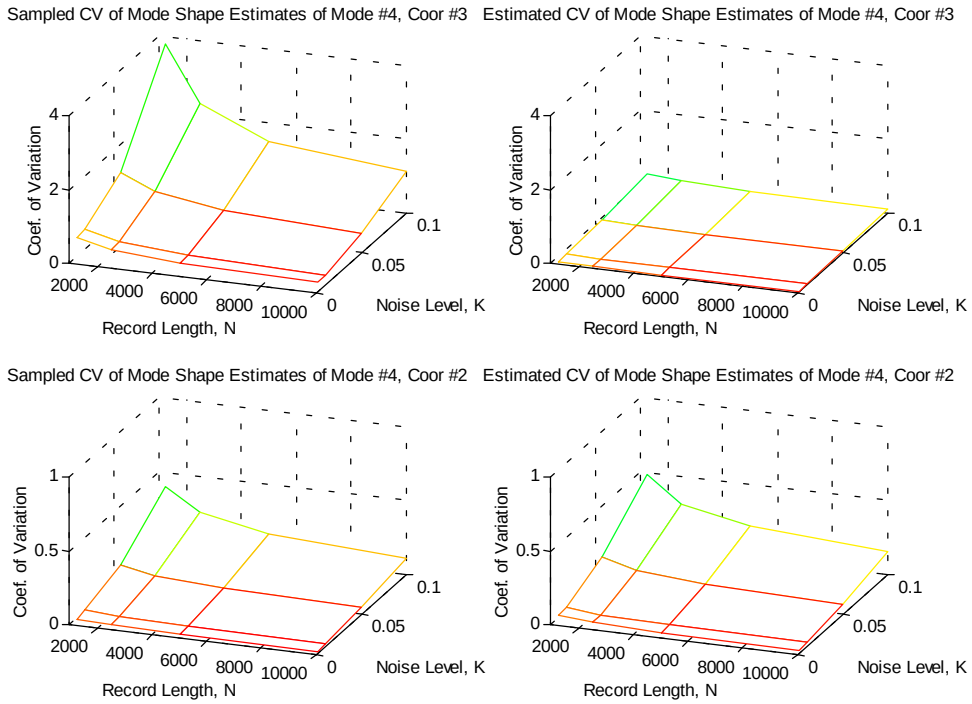

Figure 8.31: Sampled and estimated coefficients of variation for the estimates of the mode shape coordinates 3 and 2 of the fourth mode.

	$K = 0.001$	$K = 0.01$	$K = 0.05$	$K = 0.1$
$N = 1250$	9.2×10^{-1}	9.2×10^{-1}	9.1×10^{-1}	9.2×10^{-1}
$N = 2500$	9.2×10^{-1}	9.2×10^{-1}	9.1×10^{-1}	9.2×10^{-1}
$N = 5000$	9.1×10^{-1}	9.1×10^{-1}	9.1×10^{-1}	9.1×10^{-1}
$N = 10000$	9.2×10^{-1}	9.2×10^{-1}	9.1×10^{-1}	9.2×10^{-1}

Table 8.29: Normalized differences of sampled and estimated coefficients of the variation of estimated mode shape coordinate 3 of the fourth mode.

	$K = 0.001$	$K = 0.01$	$K = 0.05$	$K = 0.1$
$N = 1250$	-4.3×10^{-1}	-4.0×10^{-1}	-3.8×10^{-1}	-2.1×10^{-1}
$N = 2500$	-2.9×10^{-1}	-3.4×10^{-1}	-3.7×10^{-1}	-2.2×10^{-1}
$N = 5000$	-4.4×10^{-1}	-4.7×10^{-1}	-4.2×10^{-1}	-3.3×10^{-1}
$N = 10000$	-3.7×10^{-1}	-3.5×10^{-1}	-3.7×10^{-1}	-4.5×10^{-1}

Table 8.30: Normalized differences of sampled and estimated coefficients of the variation of estimated mode shape coordinate 2 of the fourth mode.

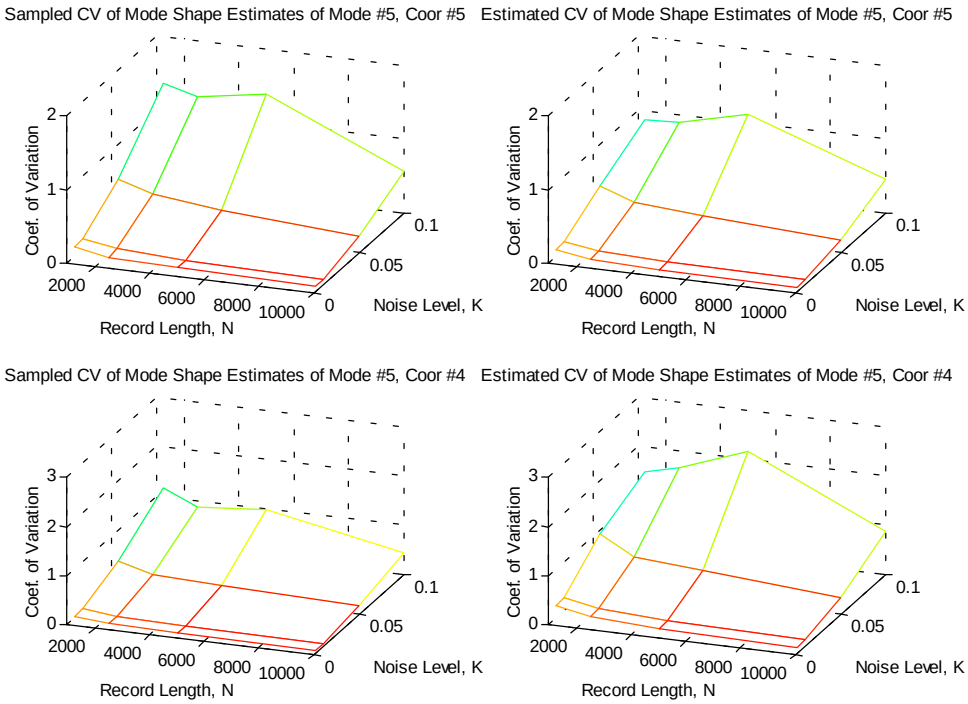

Figure 8.32: Sampled and estimated coefficients of variation for the estimates of the mode shape coordinates 5 and 4 of the fifth mode.

	$K = 0.001$	$K = 0.01$	$K = 0.05$	$K = 0.1$
$N = 1250$	1.7×10^{-1}	1.3×10^{-1}	1.3×10^{-1}	3.6×10^{-1}
$N = 2500$	1.3×10^{-1}	1.8×10^{-1}	2.4×10^{-1}	2.8×10^{-1}
$N = 5000$	2.0×10^{-1}	1.6×10^{-1}	2.3×10^{-1}	2.0×10^{-1}
$N = 10000$	1.5×10^{-1}	1.5×10^{-1}	2.0×10^{-1}	2.0×10^{-1}

Table 8.31: Normalized differences of sampled and estimated coefficients of the variation of estimated mode shape coordinate 5 of the fifth mode.

	$K = 0.001$	$K = 0.01$	$K = 0.05$	$K = 0.1$
$N = 1250$	-1.2×10^{-0}	-1.2×10^{-0}	-1.1×10^{-0}	-2.8×10^{-1}
$N = 2500$	-1.3×10^{-0}	-1.3×10^{-0}	-1.2×10^{-0}	-8.9×10^{-1}
$N = 5000$	-1.1×10^{-0}	-1.2×10^{-0}	-1.1×10^{-0}	-1.2×10^{-0}
$N = 10000$	-1.2×10^{-0}	-1.2×10^{-0}	-9.5×10^{-1}	-9.9×10^{-1}

Table 8.32: Normalized differences of sampled and estimated coefficients of the variation of estimated mode shape coordinate 4 of the fifth mode.

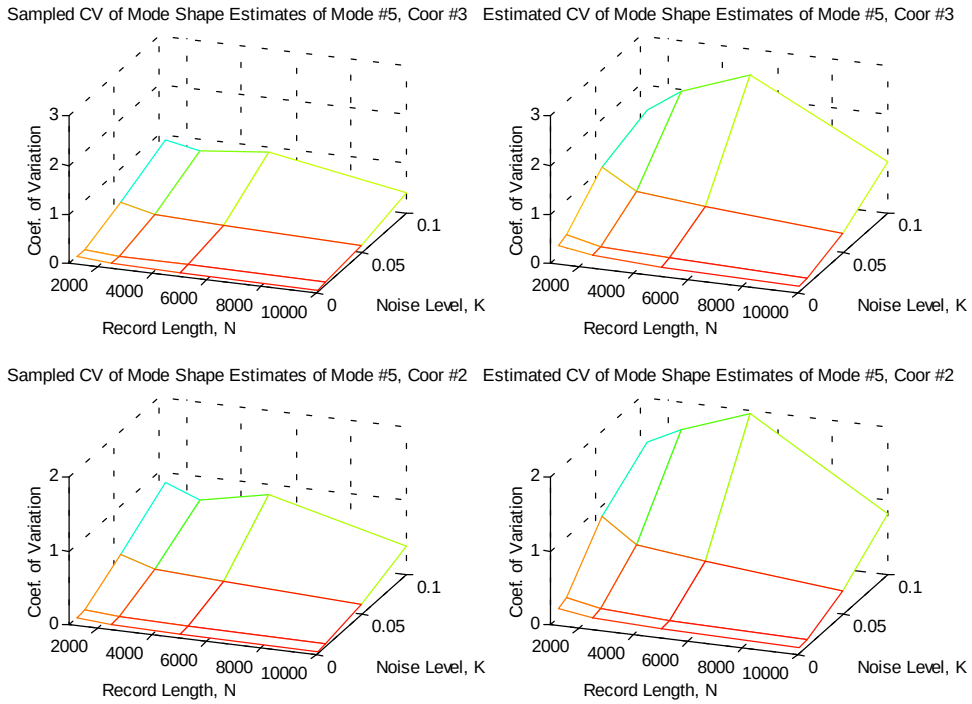

Figure 8.33: Sampled and estimated coefficients of variation for the estimates of the mode shape coordinates 3 and 2 of the fifth mode.

	$K = 0.001$	$K = 0.01$	$K = 0.05$	$K = 0.1$
$N = 1250$	-1.8×10^{-0}	-1.8×10^{-0}	-1.6×10^{-0}	-6.4×10^{-1}
$N = 2500$	-1.9×10^{-0}	-1.9×10^{-0}	-1.8×10^{-0}	-1.6×10^{-0}
$N = 5000$	-1.8×10^{-0}	-1.8×10^{-0}	-1.7×10^{-0}	-1.7×10^{-0}
$N = 10000$	-1.8×10^{-0}	-1.8×10^{-0}	-1.5×10^{-0}	-1.5×10^{-0}

Table 8.33: Normalized differences of sampled and estimated coefficients of the variation of estimated mode shape coordinate 3 of the fifth mode.

	$K = 0.001$	$K = 0.01$	$K = 0.05$	$K = 0.1$
$N = 1250$	-1.3×10^{-0}	-1.3×10^{-0}	-1.2×10^{-0}	-6.4×10^{-1}
$N = 2500$	-1.4×10^{-0}	-1.5×10^{-0}	-1.2×10^{-0}	-1.4×10^{-0}
$N = 5000$	-1.3×10^{-0}	-1.3×10^{-0}	-1.2×10^{-0}	-1.3×10^{-0}
$N = 10000$	-1.3×10^{-0}	-1.3×10^{-0}	-1.2×10^{-0}	-1.2×10^{-0}

Table 8.34: Normalized differences of sampled and estimated coefficients of the variation of estimated mode shape coordinate 2 of the fifth mode.

Separate conclusions concerning the estimation of the uncertainties of the modal parameters will be given in the following. These will primarily be based on the normalized differences of the sampled and estimated coefficients of variation presented in the previous tables.

When the number of simulations tends to infinity the sampled coefficient of variation will approach the theoretical one. This is the reason why the difference $|\nu_k - \hat{\nu}_\kappa|$ has been normalized with respect to ν_k. Thus, the estimated coefficient of variation will be compared to the sampled coefficient of variation.

If the normalized differences are positive it implies that the uncertainty of the modal parameter is underestimated, whereas it is overestimated if the normalized difference is negative. If the normalized difference is numerically less than 10^{-2}-10^{-3}, the sampled and estimated coefficient of variation agrees with 2-3 decimals. An agreement of this size will probably be adequate in applications such as VBI, see chapter 9.

Conclusions on the Natural Eigenfrequency Estimates

The figures 8.19 to 8.23 as well as the tables 8.5, 8.7, 8.9, 8.11 and 8.13 reveal a good agreement between the sampled and estimated coefficients of variation of the estimated natural eigen-frequencies. The eigenfrequencies are all very accurately determined, which is underlined by both the sampled and estimated coefficients of variation which range from 1.0×10^{-4} to 1.0×10^{-3} for the long records.

If the record length is short and the noise level is high the normalized difference is seen to be up to 10^{-1}. However, if the record length is long and the noise level is small the agreement between the sampled and the estimated coefficients of variation improves up to 10^{-3}. In this case the sampled and estimated standard deviation will agree very well.

Only in 20% of the simulation cases the normalized difference is negative. This implies that the estimated standard deviations of the natural eigenfrequency estimates tend to be too small. However, this underestimation is very small for long record lengths and moderate noise levels.

Finally, it is observed that the coefficient of variation seems to keep on descreasing as the number of samples tends to infinity. This is observed for all levels of noise.

Conclusions on the Damping Ratio Estimates

Again, the figures 8.19 to 8.23 and the tables 8.6, 8.8, 8.10, 8.12 and 8.14 reveal a good agreement between the sampled and estimated coefficients of variation of the estimated damping ratios.

However, the damping ratios are not so accurately determined as the natural eigen-frequencies. The range of both the sampled and the estimated coefficients of variation is 0.1-0.2 for the long records.

Except for the very short record lengths and high noise levels where the normalized difference is seen to be up to 10^{-1}, the normalized difference ranges from 10^{-2} to 10^{-3}. It does not seem to help significantly if the record length is increased, nor if the noise level is decreased. In other words, increasing the record length does not seem to improve the estimated coefficients of variation.

Only in 26% of the simulation cases the normalized difference is negative. This implies that the estimated standard deviations of the damping ratio estimates tend to be too small.

Finally, when the record length becomes moderate the decrease of the coefficient of variation seems to saturate. This is especially true for the low noise levels.

Conclusions on the Mode Shape Estimates

From the figures 8.24 to 8.33 and the tables 8.15 to 8.34 the coefficients of variation are presented for the coordinates 5 to 2 of the five modes. The agreement between the sampled and estimated coefficients of variation of the estimated mode shape coordinates is not so good as for the natural eigenfrequencies and the damping ratios.

The numerical values of the normalized difference of the sampled and estimated coefficients of variation are more or less constant with values around 10^{-1}. This indicates that it is impossible to improve the estimated standard deviations of the mode shape estimated by increasing the record length. Further, in 50% of the simulation cases the normalized difference is negative, which means that it is impossible to conclude whether the standard deviations will be underestimated or not. The conclusion is therefore, that the estimated standard deviation of the mode shapes must be interpreted with care.

It might be claimed that the choice of normalization coordinate plays a role. However, if this is the case the normalized differences should deviate more from mode shape to mode shape. This is not the case. However, the influence of the choice of normalization should be investigated in future work.

8.4 General Conclusions

The results of the analysis of the standard deviations of the modal parameter estimates indicate that the estimator probably becomes efficient as the record length tends to infinity. This is underlined by the bias analysis of the modal parameter estimates.

The bias of the natural eigenfrequency and damping ratio estimates decreased rapidly until a record length of 5000 samples. This was experienced for all levels of noise. The mode shapes decreased more slowly especially for high levels of noise. But in any case, the bias keept on decreasing as the number of samples was increased.

The achievable accuracy of estimated ARMA models has been investigated in e.g. Gersch [26], Jensen et al. [45] and Kirkegaard [52] and they have made the following conclusions :

- *The uncertainty of the modal parameters is relatively insensitive with respect to the number of degrees of freedom*, Gersch [26].

- *In practice, for a given level of damping, only limited improvement in the accuracy of the damping ratios estimates is obtained by increasing the record length N when N has obtained a given magnitude*, Jensen et al. [45].

- *The optimal choice of N can in principle only be evaluated by a cost-benefit analysis,* Jensen et al. [45] *and* Kirkegaard [52].

- *By choosing the record length large enough, the uncertaities of the natural eigenfrequencies and the damping ratios can be quantified,* Jensen et al. [45].

- *The accuracy of the estimated natural eigenfrequencies will increase but the accuracy of the damping ratios will decrease for decreasing levels of damping,* Jensen et al. [45].

So in conclusion :

- *For record lengths over 5000 samples in each channel and for a noise level K below 1% the standard deviations of the natural eigenfrequencies and the damping ratios can be quantified accurately and the bias will be insignificant.*

The standard deviations of the mode shapes will be more inaccurately estimated and care must be taken in interpreting these. The bias of the mode shapes will keep on decreasing even for very long records.

8.5 Summary

As described in section 1.7.1, the intention of this simulation study has been to assess the statistical properties of the PEM estimate of an ARMAV model. If the true system can be contained in the model structure and if the prediction error is Gaussian white noise, then the PEM estimator will be efficient. In this case the estimate will be asymptotically unbiased and the estimated standard deviations of the estimated modal parameters will attain the Cramer-Rao lower bound.

At the beginning of section 8.3, it was established that the ARMAV(2,2) model used in the estimation was an adequate model. This implies that the true system can be contained in it. It has been verified that the prediction errors are realizations of a multivariate Gaussian white noise process. It has also been verified, that the number of simulations is adequate in order to obtain convergent statistical properties of the estimated modal parameters.

It is concluded that for record lengths over 5000 samples in each channel and for a noise level K below 1% the standard deviations of the natural eigenfrequencies and the damping ratios can be quantified accurately and the bias will be insignificant. However, the standard deviations of the mode shapes will be more inaccurately estimated and care must be taken in interpreting these. The bias of the mode shapes will keep on decreasing even for very long records.